Single-phase mixed convective heat transfer and pressure drop in the laminar and transitional flow regimes in smooth inclined tubes heated at a constant heat flux

JP Meyer*, AI Bashir and M Everts
Department of Mechanical and Aeronautical Engineering, University of Pretoria,
Pretoria, 0002, South Africa.
*Author for correspondence, e-mail: josua.meyer@up.ac.za

Highlights

- Laminar flow heat transfer and pressure drop in inclined tubes.
- Laminar Nusselt number and friction factor correlations for inclined tubes.
- Upward and downward flow heat transfer and pressure drop.
- Influence of tube inclination on the boundaries of transitional flow regime.
- Transition gradients increases with inclination angle.

Abstract

Heat transfer and pressure drop experiments were conducted in the laminar and transitional flow regimes at different inclination Grashof numbers that generated different levels of buoyancy. A wide range of Grashof numbers were covered by varying both the inclination angle and heat flux. The experiments were conducted on an experimental set-up on which flow could occur through a smooth tube positioned at different inclination angles, from vertical downward (–90º) flow to vertical upward (+90º) flow. The test section had an internal diameter of 5.1 mm, length of 4.6 m and a square-edged inlet was used. The experiments were conducted at different inclination angles between Reynolds numbers of 1 000 and 6 000 at heat fluxes of 4 to 8 kW/m^2. The test fluid was water and the Prandtl numbers varied from 3 to 7. It was found that an increase in the inclination angle from horizontal flow (0º) to vertical (±90º) flow, decreased the buoyancy effects which led to decreased laminar heat transfer coefficients and friction factors for both upward and downward flows. The onset of buoyancy effects was significant near the vertical inclinations and caused a rapid increase in the laminar heat transfer coefficients and friction factors when the inclination angles moved from vertical to horizontal orientations. An inclined tube Grashof number which is a function of inclination angle was defined and used to express the laminar Nusselt numbers as a forced convection part plus an enhancement component owing to mixed convection. The laminar

friction factors were expressed as a function of forced convection/isothermal part multiplied by the mixed convection part. Furthermore, it was found that the critical Reynolds numbers at which transition started increased as the inclination angles increased from horizontal to vertical, while the end of transition were inclination angle independent. This caused the width of the transitional flow regime to decrease, as well as the transition gradients to increase, with increasing inclination angle at different heat fluxes. It was also found that the flow directions (upward and downward) had a negligible effect on the heat transfer coefficients and friction factors in the entire transition and quasi-turbulent regions.

Keywords: Buoyancy; inclination; heat transfer; pressure drop; laminar; transition; horizontal; vertical; forced convection; mixed convection.

Graphical abstract

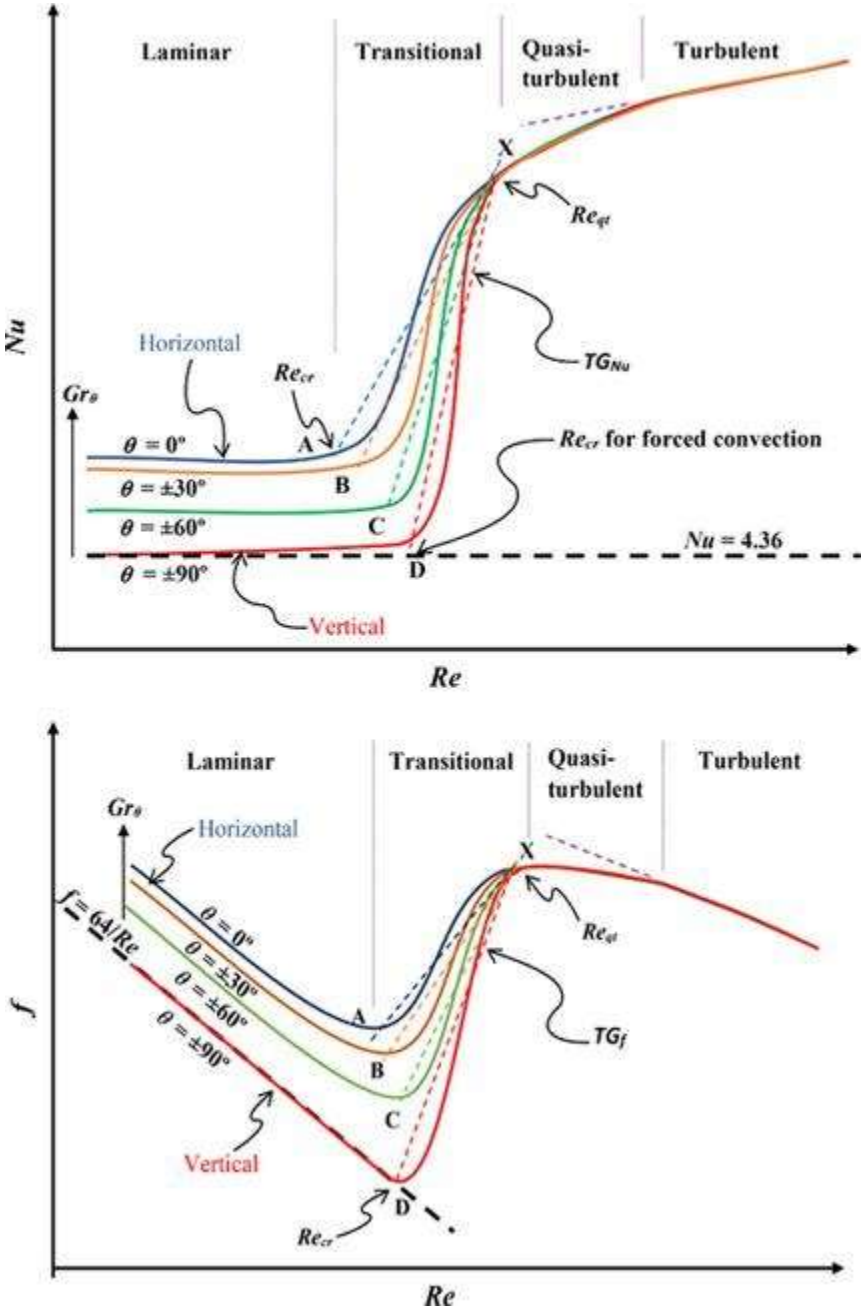

Nomenclature

b	Bulk
C	Coefficient
C_p	Specific heat at constant pressure
D	Diameter
DAQ	Data Acquisition System
DC	Direct current
eb	Energy balance error
F	Force
f	Friction factor
FCD	Forced Convection Developing
FD	Fully Developed
g	Gravitational acceleration
Gr	Grashof number
Gr^*	Modified Grashof number
Gr_θ	Inclined tube Grashof number
Gr_θ^*	Inclined tube modified Grashof number
h	Heat transfer coefficient
I	Current
i	Data point index
j	Colburn j-factor
k	Thermal conductivity
L	Length
$\dot{m}$	Mass flow rate
MCD	Mixed Convection Developing
Nu	Nusselt number
P	Pressure
Pr	Prandtl number
PT	Pressure tap
P_w	Tube wall parameter
$\dot{Q}$	Heat transfer rate
$\dot{q}$	Heat flux
R	Thermal resistance
Ra	Rayleigh Number
Ra_θ	Inclined tube Rayleigh number
Ra_θ^*	Inclined tube modified Rayleigh number
Re	Reynolds number
T	Temperature/Thermocouples
t	Tube thickness
TG	Transition gradient
V	Velocity/voltage
W	Width
x	Distance from tube inlet

Special characters

θ	Inclination angle
β	Coefficient of thermal expansion
μ	Dynamic viscosity
ρ	Density

Subscripts

avg	Average
b	Bulk/bottom
cor	Correlation
Cu	Copper
cr	Critical
e	Exit
exp	Experiment
f	Fluid/friction factor
FC	Forced convection
FD	Fully developed
$grav$	Gravity
i	Inlet/inner/data point index
iw	Inner wall
j	Colburn j-factor
MC	Mixed Convection
Nu	Nusselt number
o	Outer
$offset$	Offset at no flow conditions
ow	Outer wall
ΔP	Pressure drop
qt	Quasi-turbulent
t	Thermal/top
w	wall

1. Introduction

Heat transfer in inclined tubes has a very wide range of heat exchanger applications [1-8] such as in air-conditioning and refrigeration systems, solar energy collectors, electronic cooling equipment, automotive vehicles to aeroplanes in the transport industry, and power generation plants operated by fossil fuels, nuclear fuel or concentrated solar power.

The behaviour of convective heat transfer in inclined tubes differs from that of vertical and horizontal tubes. In vertical tubes, the buoyancy forces (free convection) acts either in the same direction (*assisting flow*) as the inertia forces or in the opposite direction to the inertia forces (*opposing flow*) [9]. In horizontal tubes, perfect laminar forced convection conditions that will ensure a Nusselt number of 4.36 for a constant heat flux, almost never occur as has been shown by Meyer and Everts [10]. It only happens when the heat fluxes are very small, and/or the tube diameters are small, and/or the fluid viscosities are high. Normally the Nusselt numbers in horizontal tubes heated at a constant heat flux are much higher than 4.36 [10-12]. The reason is that the buoyancy forces acts in a perpendicular (radial) direction to the inertia forces, producing secondary flow that significantly enhances the heat transfer, especially in the laminar flow regime.

However, in inclined tubes a combination of the heat transfer and fluid flow characteristics of horizontal and vertical tubes exist. Thus, to fundamentally understand the differences between the flow in horizontal and vertical tubes (in both upward and downward directions) it is important to investigate it in the different flow regimes at different inclination angles, from vertical downward to vertical upward.

Inclination buoyancy leads to mixed convection heat transfer, caused by the fluid density differences due to the temperature gradients between the fluid near the heated wall and the cooler fluid near the centreline. This results in increased heat transfer coefficients when compared to forced convection heat transfer coefficients. Iqbal and Stachiewicz [13] performed one of the early investigations on mixed convection heat transfer in inclined tubes. It was observed that an increase in inclination angle led to an increase in the fully developed laminar heat transfer coefficients.

Most mixed convection heat transfer analyses for inclined tubes in literature [14-22] showed that inclination buoyancy has a significant effect on the laminar heat transfer, depending on the flow direction. In general, the laminar Nusselt numbers decreased with increase in inclination angle for upward flow. This is because the components of the gravitational (buoyancy)

forces changed in the axial and circumferential direction, causing a change in Grashof numbers and thus mixed convection heat transfer. As expected, it was also found that the heat transfer increased with increasing heat flux for all inclination angles, due to the increase in the Grashof number.

Tian et al. [23] used flow visualizations to investigate the effect of buoyancy on laminar mixed convection heat transfer in inclined narrow rectangular channels with asymmetrical heating. They considered developing upward flow in near vertical inclination angles between +60º to +90º. It was found that transverse flow and buoyancy forces normal to the tube wall were the main contributing factors to mixed convection and heat transfer enhancement within the channel. A modified Grashof number correlation in terms of inclination angle, to account for buoyancy forces, in narrow rectangular channels was also developed in their part II article [24].

To account for inclination effects, Vliet [25] and Fuji and Imura [26] replaced the gravitational acceleration, g, in the buoyancy force term of the Grashof number, with the buoyancy force component parallel to the vertical surface. Rani et al. [27] developed a unified correlation for predicting natural convection heat transfer in inclined tubes. A modified Grashof number in terms of the modified characteristic length, which is a function of inclination angle, diameter and length, was used instead of the diameter or length only. However, their modified Grashof number correlation did not account for the components of the buoyancy force normal and parallel to the axis of the fluid flow.

Oosthuizen and Naylor [28] added the cross-sectional width-to-length (W/L) ratio in the Grashof number for a vertical square duct of width, W, and length, L, which can be extended to circular channels with diameter, D_i, using (D_i/L). Oosthuizen and Naylor [28] also noted that for large diameter tubes (small D_i/L), the heat transfer surface can be treated as two independent walls with separate boundary layers. However, for small diameter tubes (large D_i/L) the two boundary layers grow along the length of the tube and the flow is considered as fully developed flow when the two boundary layers meet.

Laminar mixed convection Nusselt number correlations as a function of Rayleigh number (or Grashof number) have been developed by Al-Sammarraie [14], Mohammed and Salman [15] and Orfi et al. [19] for upward flow at different inclination angles of 0º, 30º, 45º, 60º and 90º. Hence, the need to develop a single laminar Nusselt number and friction factor correlation that is valid for both upward and downward flow at all inclination angles, and also accounts for

inclination buoyancy, is paramount in the design of inclined heat exchangers. Furthermore, the aforementioned studies focused on the effect of inclination buoyancy in the laminar flow regime only, without extending the focus to the transitional flow regime.

Good progress has been made in recent years on the experimental analysis of heat transfer and pressure drop in the transitional flow regime of smooth horizontal tubes with a constant heat flux boundary condition [10, 12, 29-40]. These works focused on the influence of heating, mixed convection and inlet geometries/configurations on heat transfer and pressure drop of developing and fully developed flow in smooth horizontal tubes. Others [41-47] investigated transitional flow in horizontal tubes with a constant wall temperature boundary condition for both cooling and heating conditions. However, no work has been conducted that concentrates specifically on the transitional flow regime in inclined tubes.

Everts and Meyer [10, 12, 34, 38] investigated mixed convection heat transfer in smooth horizontal tubes in the laminar, transitional, quasi-turbulent and turbulent flow regime using two different approaches. Firstly, they compared different tube diameters, because the Grashof number, and thus buoyancy effects, is proportional to D_i^3. Similar to Ghajar and Tam [11, 29], different heat fluxes were used in the second approach. It was found that when the buoyancy effects were increased by either the tube diameter or heat flux, both the Reynolds numbers at which transition started and ended, as well as the width of the transitional flow regime and transition gradient, as defined by Everts and Meyer [12], were affected. Therefore, buoyancy effects significantly affected the heat transfer and pressure drop characteristics in the transitional flow regime. A third approach that can be used to investigate mixed convection heat transfer, is to change the inclination angle of the test section. As will be shown in this paper, different levels of buoyancy (represented by the Grashof numbers) can be generated by changing the inclination angles of a test section.

Although significant work has been done on flow through inclined tubes during phase change [1-3, 5-8, 48-50], very little has been done of the expected simpler case of single-phase flow through inclined tubes in the laminar flow regime. Specifically, there is little or no sufficient information available in literature on the method of quantifying the effect of buoyancy/mixed convection/Grashof number on the heat transfer and pressure drop in the transitional flow regime of inclined tubes. Therefore, the aim of this paper is to investigate the effect of tube inclinations and flow directions on the single-phase heat transfer and pressure drop characteristics in the laminar and transitional flow regimes of a smooth circular tube heated at constant heat fluxes.

2. Experimental set-up

Fig. 1 shows the experimental facility used to conduct the experiments for this study. Water was circulated from a 500 ℓ storage tank through flow meters, a flow-calming section and test section, and then back to the storage tank for cooling and recirculation. A chiller unit was coupled to the storage tank to cool down the heated water and maintain the water at a constant temperature.

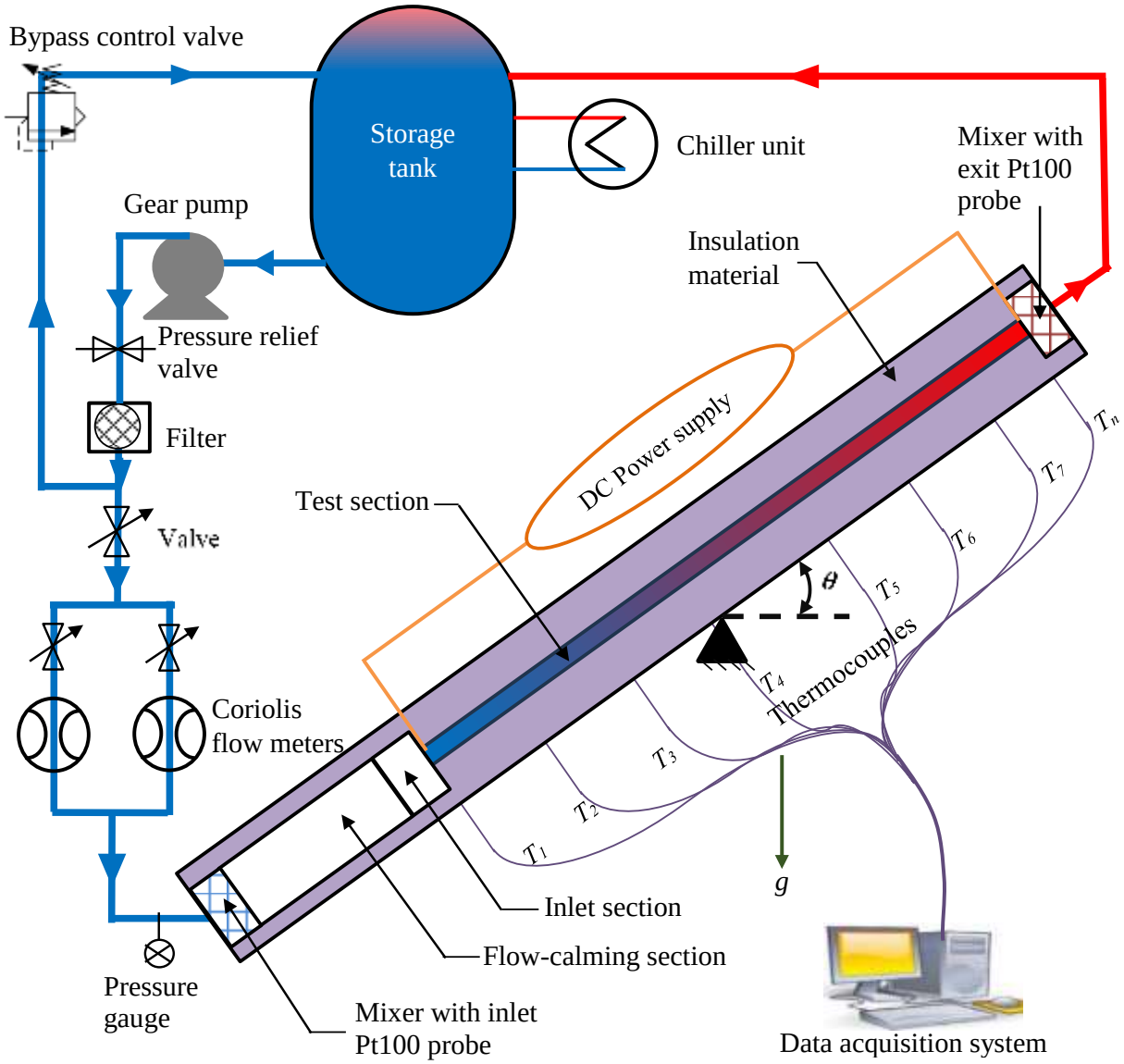

Fig. 1: Schematic layout of the experimental facility.[*]

[*] Reprinted from JP Meyer and AI Bashir, Experimental investigation of convective heat transfer in the transitional flow regime of an inclined smooth tube, in: 16th International Heat Transfer Conference, Beijing, pp. 3127-3133 (2018), with permission from Begell House.

A 420 ℓ/hr magnetic gear pump was used to circulate the water through the test section. The pump was connected to the experimental set-up using a rubber hose to prevent the transmitting of any vibrations from the pump to the test section. The pump was controlled from a personal computer and the flow rate was changed by adjusting the voltage signal sent through a Labview program. A pressure relief valve was used to bypass the water back to the storage tank when the pressure exceeded the system pressure threshold value. A water bypass line was used to increase the backpressure to avoid flow pulsations in the test section which might influence the transition characteristics [51]. A pressure gauge was used prior to the flow-calming section to monitor the pressure of the system.

The mass flow rate of the water to the test section was measured using two Coriolis flow meters with different capacities. These flow meters had an accuracy of ±0.05% of the full scale and a maximum flow rate of 330 ℓ/hr and 108 ℓ/hr respectively. The flow meter with a higher flow rate (330 ℓ/hr) was used for measurements in the quasi-turbulent and turbulent flow regimes while the smaller flow meter (108 ℓ/hr) was used for measurements in the laminar to quasi-turbulent flow regimes. The mixer design of Bakker et al. [52] with alternating right and left hand twisted helical plates, was used for both the inlet and exit mixers. The inlet Pt100 probe was installed inside a soft Nylon mesh downstream of the inlet mixer. The outlet Pt100 probe was downstream of the outlet mixer with the water stream passing along the probe in an axial direction [53].

Flow-calming section and inlet section

A flow-calming section (Fig. 2) was installed prior to the test section to ensure a uniform inlet velocity distribution to the test section. A similar design to Ghajar and Tam [29] and Tam et al. [54] was used, except that the same tube diameter was used for both the flow-calming and inlet sections to avoid any vortex occurrence caused by diameter differences. Furthermore, the contraction ratio (ratio of the inner diameter of the flow-calming section to the inner diameter of the test section) was 33; while Ghajar and Tam [29] used a contraction ratio of 10. The flow-calming section was made of clear acrylic tube with an outer diameter and length of 180 mm and 616 mm, respectively. Three air bleed valves were located at the top of the tube to remove trapped air.

Three perforated acrylic plastic plates, separated at 89 mm and 102 mm, were placed 38.1 mm from the inlet of the flow-calming section. Each acrylic plate contained 73 holes, with a

diameter of 11 mm. This was followed by tightly packed plastic straws with a diameter of 6 mm, length of 102 mm and open area ratio (OAR) of 0.92. The plastic straws were located 89 mm from the acrylic plates and were placed in-between galvanized steel wire mesh screens with an open area ratio of 0.55. Another fine steel wire mesh screen with an open area ratio of 0.45 was located approximately 25.4 mm before the outlet of the flow-calming section. The inlet section consisted of acrylic tube with a length of 235 mm and inner diameter of 172 mm. A square-edged inlet was used in this analysis.

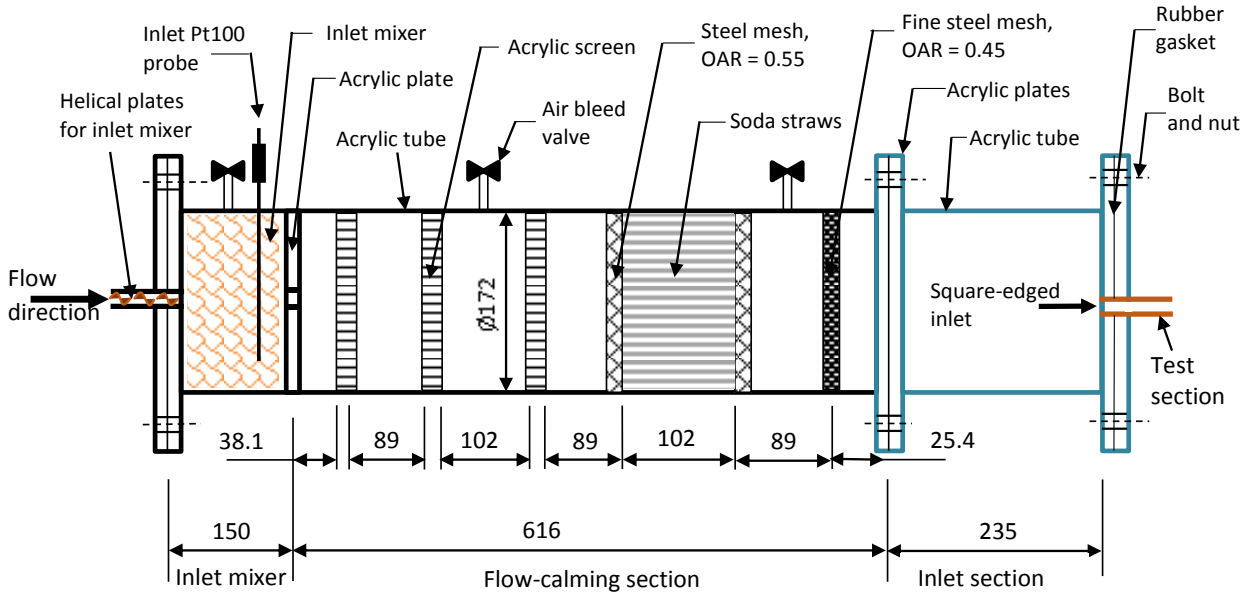

Fig. 2: The inlet mixer, flow-calming section and inlet section (all dimensions are in mm).

Test section

Fig. 3 is a schematic representation of the test section, indicating the two pressure tap locations, thermocouple stations, as well as the flow directions for the different inclination angles. The test section was made from a smooth hard drawn copper tube with measured inner and outer diameters of 5.1 mm and 6.3 mm respectively. The test section had a total measured length of 4.6 m and therefore a maximum length-to-diameter ratio (x/D_i) of 886. This length-to-diameter was much longer than that used previously in literature as discussed in Meyer and Everts [10]. The average surface roughness of the test section was measured to be approximately 0.206 µm using a surface roughness tester with a diamond stylus. The relative surface roughness was therefore 4.1×10^{-5}, and for all practical purposes, the tube can be considered as smooth.

The wall temperatures were measured at 21 thermocouple stations. As shown in Fig. 3(a), the thermocouple stations were located at closer intervals near the entrance and in the fully developed part to capture enough data in the entrance and fully developed regions. T-type thermocouples with a diameter of 0.25 mm were used. Due to the small diameter of the test section, three thermocouples were used at each station (Fig. 3(c)). One thermocouple at the top and bottom of the tube and another thermocouple alternating at the side between 90° (for station 1, 3, 5, etc.) and 270° (for station 2, 4, 6, etc.). The thermocouples were soldered to the outer surface of the tube by drilling a 0.4 mm depression and inserting a flux and solder. Heat was applied to the tube and once the solder melted, the thermocouple was inserted and the tube was allowed to cool down.

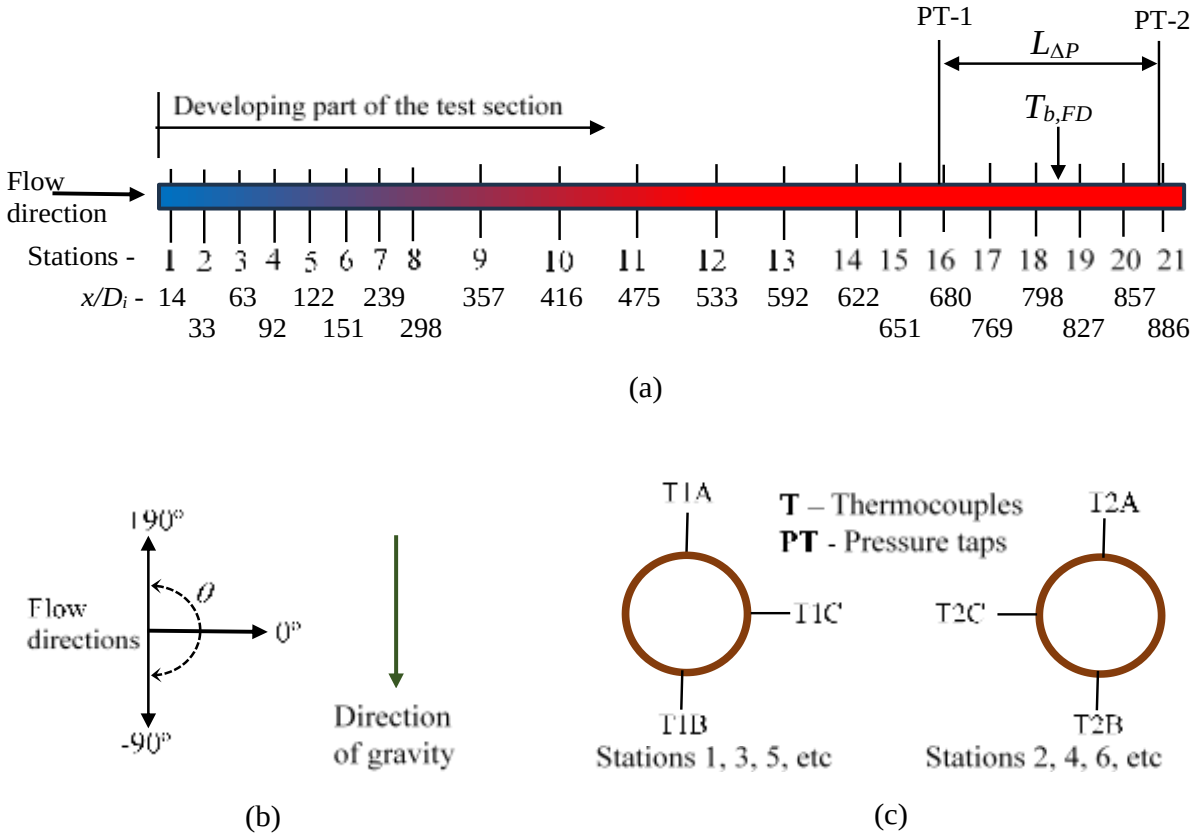

Fig. 3: Schematic representation of (a) the test section indicating the pressure taps (PT) and thermocouple stations (T), (b) the flow directions and (c) a cross section of the test section tube shows the thermocouple positions per station.[†]

[†] Adapted from JP Meyer and AI Bashir, Experimental investigation of convective heat transfer in the transitional flow regime of an inclined smooth tube, in: 16th International Heat Transfer Conference, Beijing, pp. 3127-3133 (2018), with permission from Begell House

The theoretical thermal entrance length, L_t, for forced convection was calculated to be 3.2 m (based on $L_t = 0.05 RePrD_i$ with a Reynolds number of 2 100 and a Prandtl number of 6). Therefore, conservatively the last 1.4 m of the test section always had fully developed flow and was considered as the "fully developed" part of the test section. This part was used to obtain the fully developed pressure drop and heat transfer results. For the temperature measurements the last six stations (stations 16 to 21) were used. Two pressure tap stations (PT-1 and PT-2 with length $L_{\Delta P} = 1$ m apart) were located within the fully developed region and corresponded closely to the last six temperature measuring stations.

To ensure that the pressure taps did not cause any flow obstructions within the test section, a 0.5 mm diameter hole was drilled through each pressure tap. This hole was less than 10% of the inner diameter of the tube, as suggested by Rayle [55]. The holes were properly de-burred to avoid any local increase in pressure due to presence of burrs that might have formed during the drilling process. A differential pressure transducer with an interchangeable diaphragm was connected to the pressure taps using a Nylon tube. Two different diaphragms were used for the high and low pressure drop measurements. The ranges and accuracies of all the instruments used, are given in Table 1.

Table 1: Ranges and accuracies of the instrumentation used.

Instruments	Range	Accuracy
DC power supply	0 – 1 500 W	3 W
Inclinometer	0 – 360°	0.2°
Pt100 probes	0 – 100°C	0.06°C
Thermocouples	-200 – 350°C	0.1°C
Pressure transducers	0 – 3.5 kPa	8.75 Pa
	0 – 14 kPa	35 Pa
Coriolis flow meters		
CMFS010	0 – 108 ℓ/hr	0.054 ℓ/hr
CMFS015	0 – 330 ℓ/hr	0.165 ℓ/hr

For a constant heat flux boundary condition, two T-type constantan heating wires with a diameter of 0.38 mm, were tightly coiled around the test section (skipping the thermocouple junctions) [53] and connected in parallel to a DC power supply. The two heating wires were connected in opposite polarities to avoid electromagnetic interferences due to the applied currents [51].

Test bench

A 6 m long test bench was designed and built to accommodate the test section together with the flow-calming section. This test bench was placed on a rigid frame with a height of 3 m. Damping pads were used to avoid vibration from the floor and the equipment to the test section. The test bench was pivoted at the centre and supported at both ends so that it can be orientated at different inclination angles, θ, from -90° downward to +90° upward. Tension cables were used to ensure that the test bench remained straight and rigid at all inclination angles. A digital inclinometer attached to the test bench was used to measure and set the required inclination angle.

Insulation

The flow-calming section, inlet section, test section, mixers and tubes were insulated to prevent heat transfer to the environment using Armaflex® insulation material with a thermal conductivity of 0.034 W/m K. The thickness of the insulation around the test section was 60 mm and the maximum heat loss was estimated with one-dimensional heat transfer calculations (taking into consideration the average measured wall and outside insulation temperature measurements and insulation resistance) to be less than 2%.

Experimental Procedure

Steady-state conditions were reached approximately two hours after the first start-up of a day. Steady-state conditions were assumed once there were no significant changes in the mass flow rates, temperatures, currents, pressure drops and the energy balance readings. The experiments were conducted by starting with the highest mass flow rate and then decreasing the mass flow rates by adjusting the pump speed in the Labview program. To minimize flow pulsations, the bypass and supply valves were continuously adjusted such that the pump can operate at higher mass flow rates. The heat flux was set from the DC power supply by applying the required voltage and current signals.

Measurements were taken at greater mass flow rate intervals in the laminar and turbulent flow regimes, but at closer intervals near and within the transitional flow regime. After each Reynolds number increment, approximately 5-10 minutes in the quasi-turbulent and turbulent flow regimes and 15-20 minutes in the laminar flow regime, were required to reach steady-state. In the transitional flow regime, fluctuations in temperature, mass flow rate, pressure drop and energy

balance were observed, therefore more time (approximately 20-30 minutes) was required to reach steady-state. Once steady-state was achieved, 400 data points were logged at a frequency of 20 Hz. These data points were then averaged to obtain one data point. The data logged included the inlet and exit temperatures, wall temperatures, ambient temperatures, mass flow rates and pressure drops. The temperature of the water in the storage tank was also monitored to ensure a constant inlet temperature.

The above procedure was repeated for different inclination angles. The inclination angle was increased at smaller increments from -90° vertically downward to +90° vertically upward. The horizontal angle was defined as 0° as shown in Fig. 3(b). Once the test bench was set to the required inclination angle, a strong locking mechanism was used to ensure that the inclination angle does not change during experiments. All the data obtained were saved and used in a separate program for the analysis.

Experimental test matrix

Table 2 summarizes the matrix of experiments captured at various inclination angles between -90° to +90°. A total of 1 139 mass flow rate measurements, 76 505 temperature measurements and 1 139 pressure drop measurements were conducted at 15 different inclination angles. In general, heat fluxes of 4, 6 and 8 kW/m^2 were used at all the different inclination angles, except for an additional case where a very small heat flux of 280 W/m^2 was used for forced convection validation purposes. The last row of values in Table 2 was for isothermal flow conditions; thus, no heating was applied and the results were used for the isothermal pressure drop validation and comparison.

It should be noted that the database (summarized in Table 2) collected for this study is approximately at least one to two orders of magnitude larger than that of previous studies for (vertical and inclined tubes) that varied from 36 [14] – 4 200 [56] temperature measurements, 5 [57] – 44 [58] pressure drop measurements, 2 [18] – 98 [15] mass flow rate measurements and 4 [14, 15, 17, 18] inclination angles. It can therefore be expected that with our big data base it will be possible to generate much more phenomena than what was identified previously.

Table 2: Experimental test matrix.

Inclination angle	Heat flux [kW/m^2]	Reynolds number range	Revised Grashof number, Gr_θ, range	Mass flow rate measurements	Temperature measurements[a]	Pressure drop measurements
+90°	4	1 086 – 5 892	$406 \leq Gr \leq 12\,719$	38	2 470	38
	6	1 571 – 5 778	$748 \leq Gr \leq 20\,139$	36	2 340	36
	8	2 153 – 5 985	$1\,077 \leq Gr \leq 24\,426$	36	2 340	36
+89°	6	1 495	335	1	65	1
+85°	6	1 484 – 5 708	65 – 1 613	35	2 275	35
+80°	6	1 507 – 443	134 – 2 735	32	2 080	32
+60°	4	1 084 – 5 588	215 – 4 875	39	2 535	39
	6	1 452 – 5 977	353 – 8 100	37	2 405	37
	8	1 928 – 5 822	540 – 9 982	38	2 470	38
+30°	4	1 106 – 5 818	371 – 7 058	39	2 535	39
	6	1 488 – 5 881	589 – 11 900	38	2 470	38
	8	1 950 – 5 859	972 – 15 906	36	2 340	36
0°	0.28[b]	256 – 720	161 – 180	6	390	6
	4	1 057 – 6 078	404 – 8 011	38	2 470	38
	6	1 451 – 6 082	677 – 14 235	36	2 340	36
	8	1 946 – 5 886	1 116 – 18 040	34	2 210	34
-30°	4	1 091 – 5 892	352 – 6 802	34	2 210	34
	6	1 423 – 5 709	646 – 12 678	35	2 275	35
	8	1 986 – 5 558	998 – 15 129	32	2 080	32
-60°	4	1 094 – 5 509	224 – 4 350	35	2 275	35
	6	1 512 – 5 616	359 – 7 361	34	2 210	34
	8	2 004 – 5 859	561 – 9 762	31	2 015	31
-80°	6	1 511 – 5 163	147 – 2 611	32	2 080	32
-85°	6	1 504 – 5 977	62 – 1 472	35	2 275	35
-87°	6	1 500	938	1	65	1
-88°	6	1 498	648	1	65	1
-89°	6	1 497	335	1	65	1
-90°	4	1 092 – 6 097	$397 \leq Gr \leq 12\,309$	37	2 405	37
	6	1 576 – 5 874	$777 \leq Gr \leq 21\,343$	37	2 405	37
	8	2 150 – 5 887	$1\,145 \leq Gr \leq 23\,602$	33	2 145	33
0°, ±30°, ±60°, ±90°	0[c]	1 000 – 6 000	-	280	18 200	280
Total				1 139	76 505	1 139

[a] Three thermocouples per station and two Pt100 probes (inlet and exit bulk temperatures).

[b] Heat flux for forced convection validation experiments.

[c] Isothermal experiments with no heating which were used for pressure drop validation experiments.

3. Data reduction

Over the tube with measured length, L, the fluid temperatures, $T(x)$, at any axial position, x, were determined from the measured inlet, T_i, and exit, T_e, fluid temperatures as obtained from the two Pt100 probes located at the inlet and outlet of the test section:

$$T(x) = T_i + \frac{(T_e - T_i)x}{L} \tag{1}$$

Thus, linear temperature profiles were assumed for the temperatures as constant heat fluxes were applied to the test section. The bulk temperature for the *fully developed* part of the test section ($T_{b,FD}$ in Fig. 3) was determined at the measured distance x = 3.92 m from the inlet as shown in Fig. 3(a). This temperature was thus measured at the centre of the two pressure taps. Depending on what was required (fully developed bulk values or local values) these temperatures were also used to determine all the fluid properties (densities, ρ, viscosities, μ, Prandtl numbers, Pr, specific heat values, C_p, and volume expansion coefficients, β) using the correlations of Popiel and Wojtkowiak [59] for water.

The single-phase pressure drops were estimated using a similar approach to previous work [60-65]. The friction pressure drops, ΔP_f, used to calculate the friction factors were obtained as follows:

$$\Delta P_f = \Delta P_{exp} - \Delta P_{grav} \tag{2}$$

ΔP_{exp}, was the measured pressure drops, $\Delta P_{measured}$, obtained from the differential pressure transducers at different inclination angles that were corrected by the pressure offset, ΔP_{offset} at no flow condition to account for the vertical height ($L_{\Delta P}\, sin\theta$ in Fig. 3) pressure difference between the pressure taps at isothermal conditions:

$$\Delta P_{exp} = \Delta P_{measured} + \Delta P_{offset} \tag{3}$$

When heat was applied at different inclination angles, the gravitational pressure drops, ΔP_{grav} in Eq. (2), were due to density difference with and without heating (due to temperature gradients) and were defined as the pressure difference between the pressure at the reference inlet

fluid temperature before heating (isothermal) and the average pressure within the heated test section (between the pressure taps):

$$\Delta P_{grav} = \rho_{b,FD} g L_{\Delta P} sin\theta - \rho_i g L_{\Delta P} sin\theta = \left(\rho_{b,FD} - \rho_i\right) g L_{\Delta P} sin\theta \quad (4)$$

where $\rho_{b,FD}$ and ρ_i were the bulk density obtained from the temperature at the bulk fully developed, *b,FD* station in Fig. 3(a) and the density at the inlet before the fluid is heated in the test section respectively. At the highest heat flux of 8 kW/m^2 and the lowest Reynolds number of 2 100, the fluid density changed from 997 to 988 kg/m^3 along the tube length for the +90º inclination. This change in density was sufficient to change the gravitational and frictional pressure drops, especially at low Reynolds numbers where the pressure drop was low. At these conditions, the frictional pressure drop (Eq. (2)) may change up to ±135%.

The gravitational acceleration, g, was taken as 9.81 m/s^2 and, $L_{\Delta P}$, was the measured distance between the two pressure taps (PT-1 and PT-2 in Fig. 3) which was 1.0 m. The measured inclination angles, θ, were measured from the horizontal plane and upward fluid flows were defined as having a positive value for, θ, while downward flows were defined as having negative signs. Thus, for vertical upward and downward flows inclination angles of θ = +90° and θ = -90° were used respectively, while θ = 0° was used for horizontal flow.

The friction factors, f, were obtained from the calculated frictional pressure drops, ΔP_f, as follows:

$$f = \frac{2\Delta P_f D_i}{L_{\Delta P} \rho_{b,FD} V_{avg}^2} = \frac{\Delta P_f \rho_{b,FD}\, \pi^2 {D_i}^5}{8 L_{\Delta P} \dot{m}^2} \quad (5)$$

The local or bulk fully developed Reynolds numbers were calculated from the measured mass flow rates:

$$Re = \frac{4\dot{m}}{\pi D_i \mu} \quad (6)$$

with the viscosities, μ, determined at the local mean fluid temperature, $T(x)$, or at the bulk fully developed, *b,FD* temperature station as shown in Fig. 3(a).

The heat transfer rates, $\dot{Q}_f$, to the fluid were determined from the measured mass flow rates, $\dot{m}$, and the difference between the measured inlet and exit fluid temperatures:

$$\dot{Q}_f = \dot{m} C_p (T_e - T_i) \tag{7}$$

The energy balance error, *eb*, was used to compare the measured heat transfer to the water, $\dot{Q}_f$, with the electrical energy supplied, $\dot{Q} = IV$, and is given as:

$$eb = \left[\frac{\dot{Q} - \dot{Q}_f}{\dot{Q}}\right] \times 100 \tag{8}$$

where *I* and *V* were the measured currents and voltage drops.

The heat flux applied to the fluid, $\dot{q}_f$, was calculated as follows:

$$\dot{q}_f = \frac{\dot{Q}_f}{\pi D_i L} \tag{9}$$

The heat transfer rate to the fluid, $\dot{Q}_f$, was used to determine the heat flux rather than the electrical power supplied, $\dot{Q}$, as the electrical power supplied was always a little larger than the heat transfer rate to the water, $\dot{Q}_f$, because of the heat losses from the test section. These heat losses were on average 2.5% and corresponded well to the theoretical determined heat losses taking into consideration the resistance of the insulation material, average measured wall temperatures and the measured temperatures on the outside of the insulation wall.

The local heat transfer coefficients at any axial point, x, from the tube inlet were determined as:

$$h = \frac{\dot{q}_f}{T_{iw} - T(x)} \tag{10}$$

where $T(x)$ was obtained from Eq. (1) and T_{iw} was the inner wall temperature obtained by taking into consideration the tube thermal resistance, R_w, as:

$$T_{iw} = T_{ow} - \dot{Q}_f R_w \tag{11}$$

The outside wall temperatures, T_{ow}, were obtained from the wall temperature measurements at each station and were the average of the three thermocouple measurements at each station. The tube thermal resistance, R_w, was determined as:

$$R_w = \frac{ln(D_o/D_i)}{2\pi k_w L} \tag{12}$$

where D_o (6.3 mm) and D_i (5.1 mm) were the measured tube outer and inner diameters and k_w the thermal conductivity of the copper tube which was 401 W/m.K [9].

These calculations showed that the temperature differences between the inside and outside walls were negligible and much smaller than the errors of the thermocouple measurements. Although these differences were taken into consideration in this study, for all practical purposes it could be assumed that the inner wall temperatures were equal to the measured outside wall temperatures.

From the local heat transfer coefficients, the local Nusselt numbers were calculated as:

$$Nu = \frac{hD_i}{k} \tag{13}$$

The average Nusselt numbers of the fully developed part of the test section from x = 3.47 m (station 16 in Fig. 3) to x = 4.52 m (station 21) were obtained from calculating the averages of the local Nusselt numbers at the last six measuring stations.

Also determined were the Colburn j-factors:

$$j = \frac{Nu}{RePr^{\frac{1}{3}}} \tag{14}$$

and the Grashof number, Gr, as:

$$Gr = \frac{g\beta\rho^2\left(T_w - T(x)\right){D_i}^3}{\mu^2} \tag{15}$$

as well as the modified bulk Grashof number, Gr^*, in terms of heat flux:

$$Gr^* = \frac{g\beta\rho^2\dot{q}_f {D_i}^4}{k\mu^2} \tag{16}$$

The average values of the Grashof numbers over the fully developed part of the test section were determined by averaging the last six values.

The width of the transitional flow regime, ΔRe, and the transition gradient of the Colburn *j*-factors, TG_j, as recently defined by Everts and Meyer [12], were calculated using the Reynolds numbers and Colburn *j*-factors at the start and end of the transitional flow regime:

$$\Delta Re = Re_{qt} - Re_{cr} \tag{17}$$

$$TG_j = \frac{j_{qt} - j_{cr}}{Re_{qt} - Re_{cr}} \tag{18}$$

The Reynolds number at the start of the transitional flow regime, $Re_{cr,}$ was obtained as prescribed by Everts and Meyer [12]:

$$Re = Re_{cr} \text{ when: } \left(\frac{dj}{dRe}\right)_{i-2:i} = 0 \tag{19}$$

where *i*-2:*i* means that any given point *i*, *dj/dRe* was determined from the three data points at *Re*(*i*-2), *Re*(*i*-1) and *Re*(*i*) for increasing Reynolds numbers. The Reynolds number at the end of the transitional flow regime, $Re_{qt,}$ were defined as [12]:

$$Re = Re_{qt} \text{ when: } \left(\frac{d^2Nu}{dRe^2}\right)_{i:i+2} \geq -0.00015 \tag{20}$$

where *i*:*i* + 2 means that at any given point *i*, the *dNu/dRe* was determined from the three data points at *Re*(*i*), *Re*(*i*+1) and *Re*(*i*+2) for increasing Reynolds numbers (while Eq. (19) used the results at the previous two Reynolds numbers).

4. Uncertainty

All uncertainties were estimated within a 95% confidence level as prescribed by Dunn [66]. For the uncertainty analyses of this paper, the manufacturer instrumentation errors were used as the fixed errors and two times the standard deviation of 400 data points as the random error. The

thermocouples and Pt100 probes were calibrated against a reference thermometer with an accuracy of ±0.03°C. The maximum Reynolds number uncertainty was found to be approximately 1.8%. The maximum friction factor uncertainty in the laminar region was 8.5% and it reduced to approximately 2.3% in the turbulent flow regime. In the transitional flow regime friction factor uncertainty increased to a maximum of 14%. This was due to fluctuations of the mass flow rates, temperatures and pressure drop measurements within the transitional flow regime [12].

The maximum Nusselt number uncertainties were 2.8%, 13%, and 5.8% respectively in the laminar, transitional and turbulent flow regimes at the maximum heat flux of 8 kW/m^2. Again, the higher uncertainties in the transitional flow regime were caused by the higher fluctuations in the wall and exit temperature measurements. As the inclination angle increased from horizontal (0º) flow to the maximum inclination angle (vertical flow), the maximum Nusselt number uncertainty in the laminar flow regime decreased slightly to 2.3%. This was due to increase in temperature difference between the fluid and wall temperatures as the inclination increased. The uncertainties in the turbulent flow regime at vertical flow followed a similar trend with that of horizontal flow and were approximately the same. As expected in transitional flow regime, due to the fluctuations of the measurements, the maximum Nusselt number uncertainty was 20%. Furthermore, as the heat flux decreased from 8 kW/m^2 to 4 kW/m^2, all the uncertainties increased slightly, as expected due to decrease in temperature difference between the bulk fluid and wall temperatures. For the lowest heat flux of 4 kW/m^2, the maximum Nusselt number uncertainties were 4.2%, 18%, and 12% respectively, in the laminar, transitional and turbulent flow regimes.

Although experiments were conducted at Reynolds numbers up to 6 000, the results showed that for this paper, sufficient conclusions could be made for Reynolds numbers up to 4 000. At this Reynolds number the maximum Nusselt number uncertainties at a heat flux of 6 kW/m^2 for horizontal and vertical inclination were 4.4% and 4.8% respectively. It has also been found that the Colburn *j*-factor uncertainties were for all practical purposes the same as that of the Nusselt number uncertainties.

5. Validation

Validation experiments were conducted for the smooth tube in a horizontal orientation ($\theta = 0°$ in Fig. 1) for the fully developed part of the test section. The validation experiments

consisted of isothermal friction factors, local laminar Nusselt numbers for forced and mixed convection conditions and average Colburn *j*-factors in the turbulent flow regime.

Isothermal pressure drop

The pressure drop validation considered a total of 40 data points for decreasing Reynolds numbers from 6 000 to 1 000, thus spanning over the turbulent, transitional and laminar flow regimes. The laminar and turbulent isothermal friction factors were compared with the Poiseuille [67] and Blasius [68] correlations respectively in Fig. 4. The fully developed friction factors were determined over the last part of the test section and the Reynolds number was determined at the centre between the two pressure taps (*b,FD* - station in Fig. 3(a)).

The laminar isothermal friction factors compared well with the Poiseuille correlation between Reynolds numbers of 1 000 and 2 200, with an average deviation of 2.7% and a maximum deviation of 5%. In the turbulent flow regime, the experimental data compared well with the Blasius [68] correlation between Reynolds number of 4 000 and 6 000, with an average deviation of 1% and a maximum deviation of 1.7%.

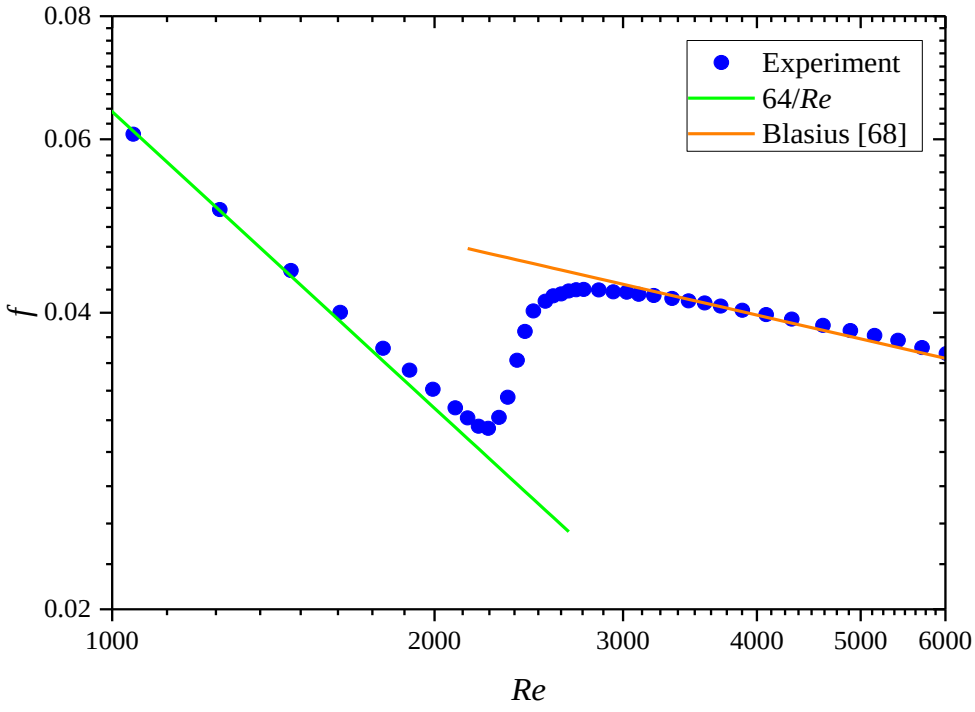

Fig. 4: Validation of the fully developed isothermal friction factors for horizontal flow with literature.

Heat transfer

The local laminar Nusselt numbers at a very small heat flux of 280 W/m^2 and a bulk fully developed Reynolds number of 660 (with a corresponding Prandtl number of 5.18) are given in Fig. 5(a). According to the newly developed flow regime map of Everts and Meyer [38], forced convection conditions were expected. Fig. 5(a) indicates that the Nusselt numbers indeed converged to the theoretical value of 4.36 for a constant heat flux boundary condition, which confirmed that the flow was dominated by forced convection.

The average Nusselt number between x/D_i = 416 and x/D_i = 857 in Fig. 5(a) was 4.39, which was within 0.7% of the value of 4.36. The last measuring points at x/D_i = 886 was excluded as it seemed as if the flow was influenced by the exit mixer. As this was also observed in previous studies [10, 12, 34-38, 40, 43-46], it is recommended for future work that the distance between the last measuring station and the tube outlet/mixer be increased.

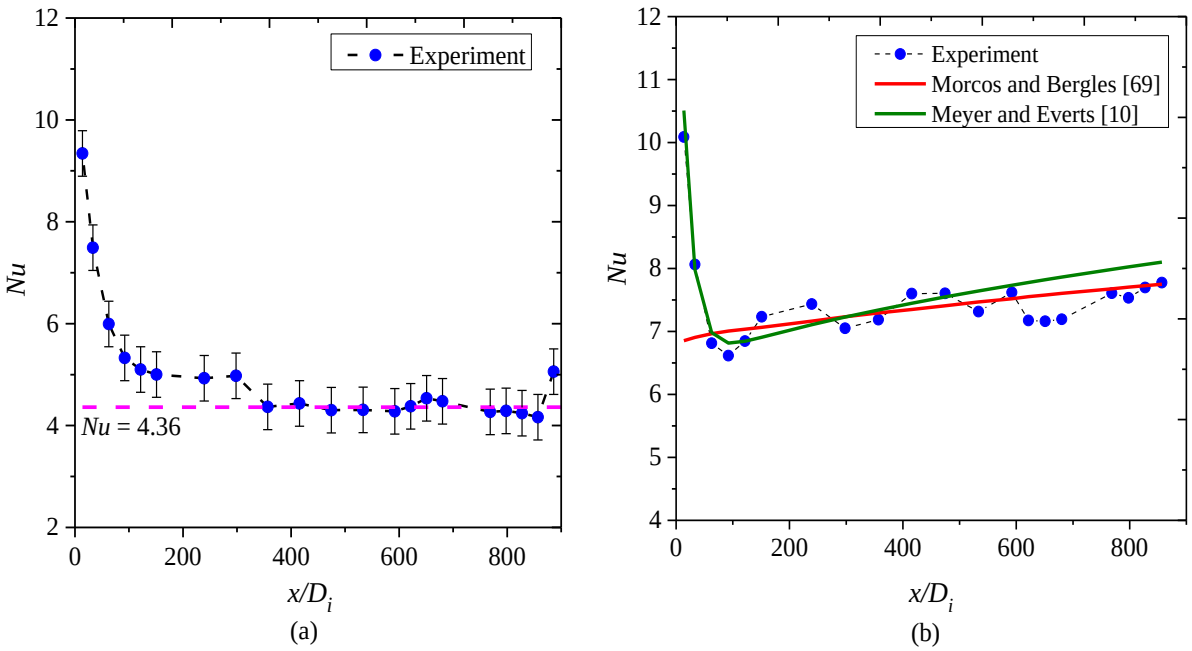

Fig. 5: Validation of the local Nusselt numbers as a function axial position for (a) forced convection conditions at a heat flux of 280 W/m^2 and bulk fully developed Reynolds number of 660 and (b) mixed convection conditions at a heat flux of 6 kW/m^2 and bulk Reynolds number of 1 450.

According to Meyer and Everts [10] a longer thermal entrance length is required when the flow is simultaneously thermally and hydrodynamically developing (as in this study), therefore a

coefficient, C, of 0.12 instead of 0.05 was suggested in the correlation $L_t=CRePrD_i$. For the conditions in Fig. 5(a), the flow was thus expected to be fully developed at x/D_i = 459. Fig. 5(a) indicates that the flow was fully developed between x/D_i =357 and x/D_i = 416, which was within 10% of x/D_i = 459. These results also show that the flow will be fully developed over the last part of the test section, between the two pressure taps PT-1 and PT-2 in Fig. 3(a). This is because the thermal entrance for forced convection is the longest and it decreased with increasing buoyancy effects (mixed convection) [10] as the inclination angle increased (as will be shown in this paper). Furthermore, it is known [9] that the hydrodynamic entrance length is less than the thermal entrance length for fluids with Prandtl numbers greater than one. It was therefore assumed that once the flow is thermally fully developed, it is also hydrodynamically fully developed.

The local Nusselt numbers at a heat flux of 6 kW/m^2, bulk Prandtl of 3.29, bulk Reynolds number 1 450, and a modified Grashof number of 109 264, were compared with the correlations of Morcos and Bergles [69] and Meyer and Everts [10] in Fig. 5(b). For all the experiments conducted, the modified Grashof numbers ranged between 2 393 and 119 452, which varied by two orders of magnitude. According to the flow regime map of Everts and Meyer [38], the flow was expected to be dominated by mixed convection. This was confirmed by the measurements, because the Nusselt numbers were much higher than 4.36. For instance, at the highest heat flux of 8 kW/m^2, the Nusselt numbers increased by 86% from the forced convection Nusselt number of 4.36, to a Nusselt number of 8.1 at horizontal orientation, which indicate a significant heat transfer enhancement due to buoyancy effects and thus mixed convection. Furthermore, the results also correlated well with the correlation of Meyer and Everts [10] with an average deviation of 4% and maximum deviation of 8%.

Although the correlation of Morcos and Bergles [69] was developed for tube wall parameters, $P_w = kD_i/(k_wt)$, between 2 and 66, it varied in this study between 0.0133 and 0.0138, which was far outside the specified range for which the correlation was developed. However, the average deviation between the experimental results and the correlation of Morcos and Bergles was 2.6%, and the maximum deviation was only 5%. It therefore seemed as if the correlation of Morcos and Bergles [69] were valid for a much wider range of tube wall parameters than they have specified. This was also found by Meyer and Everts [10].

The average Colburn j-factors of the fully developed part of the test section in the turbulent flow regime were compared with the correlations of Gnielinski [70], Ghajar and Tam [29], and the

newly developed correlations of Meyer et al. [71] in Fig. 6. The results compared well with the correlations of Gnielinski [70] and Meyer et al. [71] with average deviations of 6.1% and 5.6% respectively and maximum deviations of 13% and 8.6% respectively. The average deviation between the results and the Colburn *j*-factors predicted using the correlation of Ghajar and Tam [29] was 16%. In general, the deviations between the experimental results and literature were larger in the turbulent flow regime than in the laminar flow regimes. This was as expected, because the temperature differences between the wall and fluid decreased with increasing Reynolds number, which led to increased uncertainties.

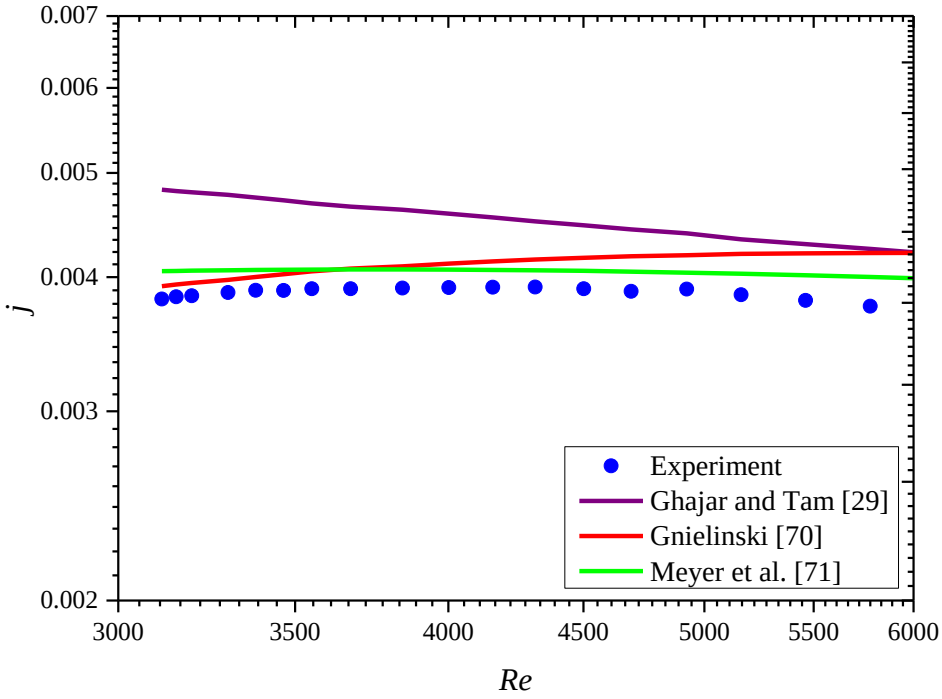

Fig. 6: Comparison of the average fully developed turbulent Colburn *j*-factors as function of Reynolds number with literature. The Colburn *j*-factors were the average over the fully developed part and the Reynolds number was determined at the *b,FD*-point identified in Fig. 3.

6. Results

The comparison of heat transfer and pressure drop results were made as function of inclination angle and the results were used to investigate the direct relationship between inclination angle and buoyancy force. The general notation in most graphs where inclination angles were used was that the square (blue) markers represented horizontal flow, while the other inclination angles were represented by solid circle markers for upward flow and empty circle markers for downward flow.

The results were always for fully developed flow, except when otherwise stated. Therefore, the Reynolds numbers were always at the *b,FD* point as shown in Fig. 3(a). Local Reynolds numbers were only used in Section (0). Most of the results (except where otherwise stated) were given at a heat flux of 6 kW/m^2 as the uncertainties at this heat flux were the lowest. The same trends were observed at the other heat fluxes as well, therefore the same conclusions could be made.

Fully developed flow pressure drop

6.1.1 Isothermal friction factors

Fig. 7 compares the isothermal fully developed friction factors as a function of Reynolds number for inclination angles from -90° (downward) to +90° (upward). For comparison purposes, the Poiseuille (64/*Re*) [67] and Blasius [68] correlations for laminar and turbulent flow respectively, were also included. As expected, Fig. 7 indicates that there were no significant differences between the friction factors obtained at different inclination angles and all the results were within the measurement uncertainties. The start and end of transition were also the same for all inclination angles. In the laminar flow regime, the magnitude of all the friction factors of the different inclinations were approximately equal and within 5% deviation from 64/*Re*. Similarly, in the quasi-turbulent and turbulent flow regimes, the friction factors of the different inclinations were all within a 1.7% deviation from the Blasius [68] correlation.

Although the uncertainties in the transitional flow regime were higher due to the mass flow rate and pressure drop fluctuations, there was no significant difference between the friction factors obtained at different inclination angles. This is because the same flow-calming section and inlet geometry were used and there were no temperature changes in the tube that could lead to buoyancy forces that influence the mechanism of transition. Transition started at a Reynolds number of approximately 2 260 for all the inclination angles. These results were as expected, but were necessary for comparison purposes.

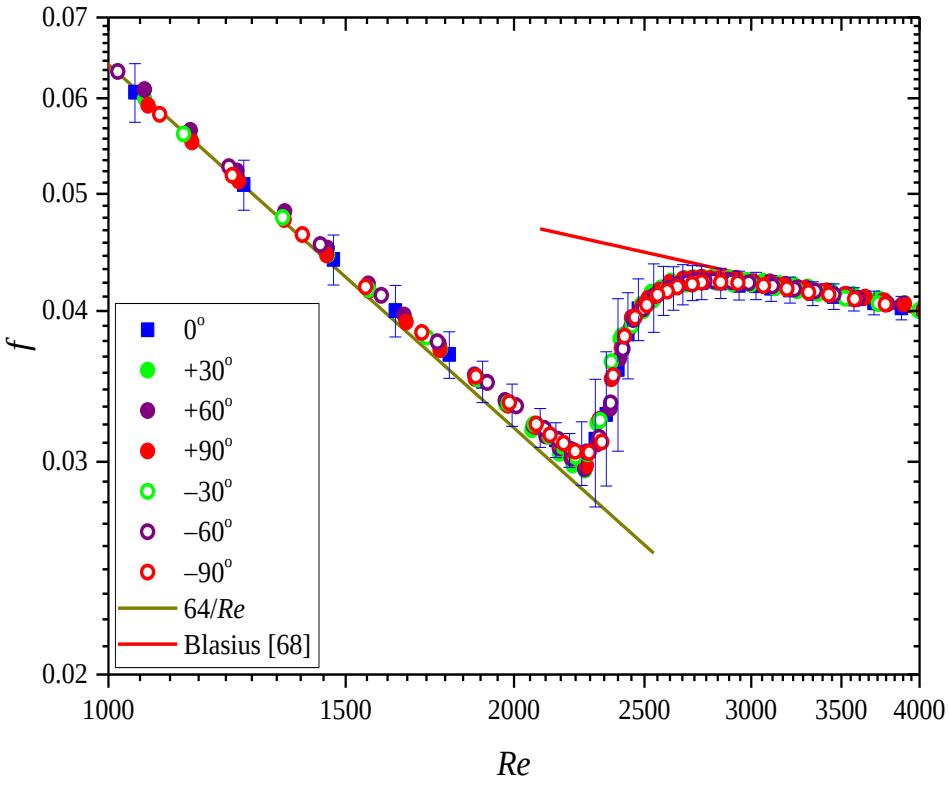

Fig. 7: Fully developed isothermal friction factors as a function of Reynolds number for different inclination angles in the upward and downward flow directions.

6.1.2 Diabatic friction factors

Fig. 8 shows the friction factors at a heat flux of 6 kW/m^2 for different inclination angles as a function of Reynolds number. In the laminar flow regime, the friction factors of horizontal flow (θ = 0°) were on average 15% higher than the Poiseuille (64/*Re*) correlation. This corresponds well to findings of Ghajar and Tam [11] and Everts and Meyer [34]. Although the viscosity shear forces on the heated wall decreased with an increase in temperature, secondary flow due to the buoyancy forces led to increased friction factors [34].

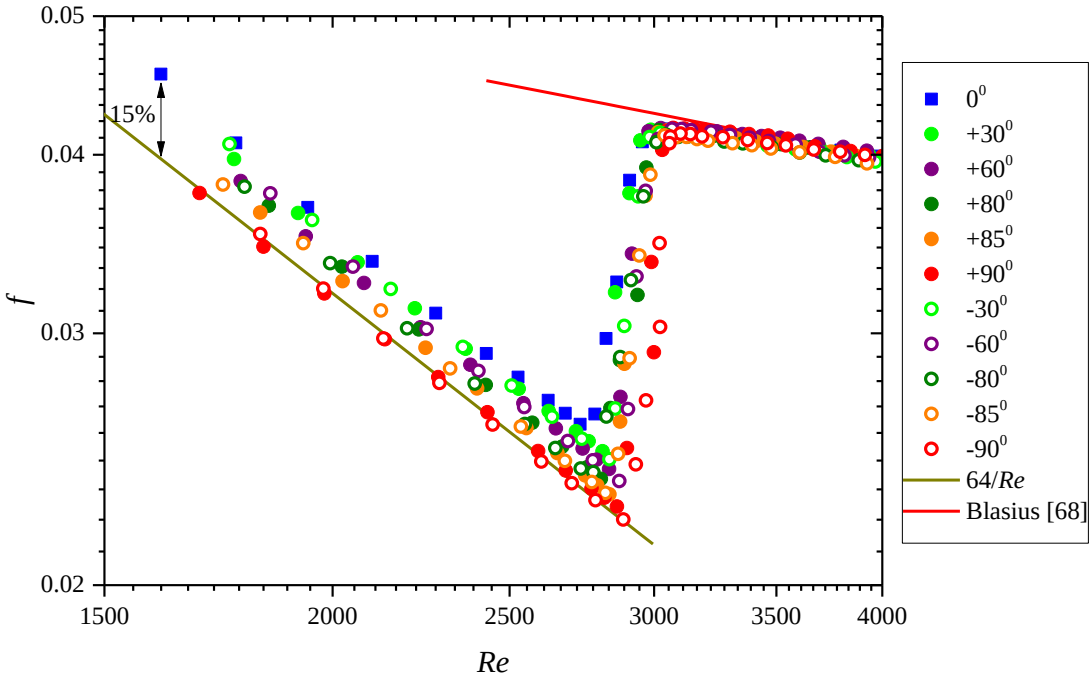

Fig. 8: Comparison of fully developed diabatic friction factors as a function of Reynolds number for different inclination angles at a heat flux of 6 kW/m^2.

Fig. 8 also indicates that the laminar friction factors decreased with the absolute value of the inclination angle, $|\theta|$, and that the friction factors were a symmetric function of inclination angle. Thus, the friction factors for an inclination angle of -30° (downward) were the same as for an inclination angle of +30° (upward). The vertical upward and downward flow friction factors were the lowest and corresponded closer to the to the forced convection friction factors predicted by the Poiseuille correlation (64/*Re*).

In Fig. 9(a), the friction factors were given as function of inclination angle for five Reynolds numbers varying from 1 800 – 2 700. For clarification, the *y*-scale scale for a Reynolds number of 2 600 has been enlarged in Fig. 9(b) to more clearly show that the friction factors for a specific negative angle, such as +30° upward, corresponded very well to the same angle of -30° downward. Furthermore, the friction factors for vertical upward flow (θ = +90°) and vertical downward (θ = -90°) flow converged to the forced convection and isothermal results of f = 64/*Re*. For flow at a specific laminar Reynolds number through a horizontal (θ = 0°) heated tube, the friction factor was significantly higher than the isothermal friction factor.

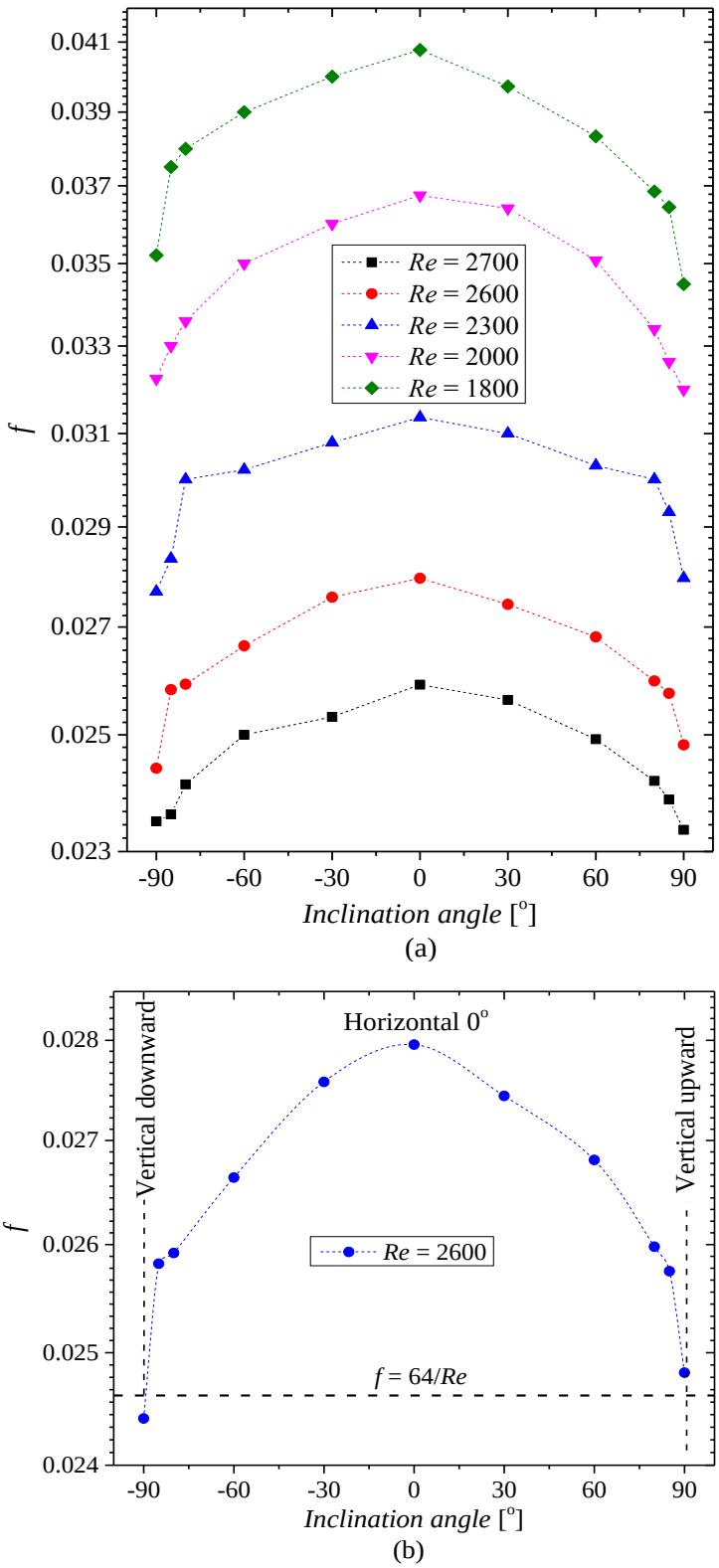

Fig. 9: Comparison of fully developed diabatic friction factors at a heat flux of 6 kW/m^2 as a function of inclination angle at (a) different Reynolds numbers and (b) Reynolds number of 2 600.

It can therefore be concluded that buoyancy effects were the greatest for the tube in a horizontal configuration ($\theta = 0°$) and decreased with changes in the inclination angle (either upward or downward inclination angle). Hence, an increase in the absolute value of the inclination angle, $|\theta|$, increased the buoyancy effects and therefore the laminar friction factors increased accordingly. Furthermore, for the purposes of this study, vertical flow (upward or downward) could be considered as pure forced convection when the Reynolds number was higher than 600 as was shown by Bashir et al. [72]. Fig. 9 also indicates that the increase in inclination from 60° to 90°, led to a greater decrease in friction factors than when the inclination angle was increased from 0° to 30°. Therefore, the decrease in the buoyancy force was more significant near vertical inclinations than near horizontal inclinations.

The Reynolds numbers at which transition started (Re_{cr}) and ended (Re_{qt}) in Fig. 8 were compared as a function of inclination angle in Fig. 10. Transition started at a Reynolds number of 2 733 for $\theta = 0°$, but was delayed to a Reynolds number of approximately 2 885 when the inclination angle was increased to vertical upward and downward flow. Although both the Reynolds numbers at which transition started and ended increased with increasing inclination angle, the increase was more for the critical Reynolds numbers (Re_{cr}). For example, the critical Reynolds number, Re_{cr}, increased with 152 from a value of 2 733 at $\theta = 0°$ to 2 885 at $\theta = \pm 90°$, while the Reynolds number at which transitions ended, Re_{qt}, increased with 45, from a value of 2 995 at $\theta = 0°$ to 3 040 at $\theta = \pm 90°$. This is because the buoyancy effects were greater at the start of transition (near the laminar flow regime) than at the end of the transition (near the quasi-turbulent flow regime). This also explains why the differences in friction factors for different inclination angles in Fig. 8 were more at the start of transition than at the end of transition.

As the flow approached the quasi-turbulent flow regime, the buoyancy effects were suppressed because of the turbulent motion of the fluid and all the transition friction factors converged to approximately the same Reynolds number of 3 040, as well as the same friction factor of 0.0412. The magnitude of the friction factors in the quasi-turbulent regime were approximately the same for all the inclination angles at any given Reynolds number.

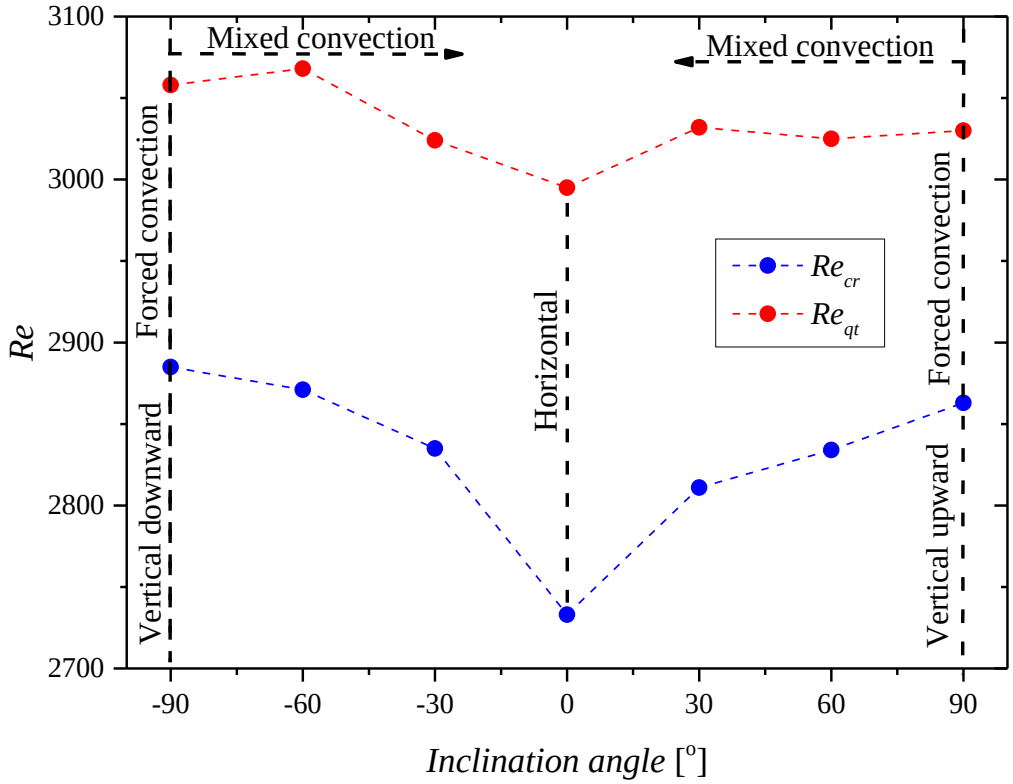

Fig. 10: Reynolds numbers at which transition started (Re_{cr}) and ended (Re_{qt}) as a function of inclination angle for the diabatic friction factors in Fig. 8 at a heat flux of 6 kW/m^2.

Fully developed flow heat transfer

6.1.3 Laminar flow

The local Nusselt numbers at different inclination angles were plotted as a function of axial location at a bulk Reynolds number of 1 600 for upward flow in Fig. 11(a) and downward flow in Fig. 11(b). The constant property forced convection Nusselt number of 4.36 for a constant heat flux is indicated by the black dotted line. In general, six conclusions can be made from Fig. 11:

(i) The flow could be considered as fully developed at $x/D_i \approx 416$. This confirmed that the flow was fully developed between the two pressure taps at $x/D_i = 680$ and $x/D_i = 886$ for the all inclination angles.

(ii) The horizontal ($\theta = 0°$) fully developed Nusselt number was 7.5 on average, which was within 4.8% of the fully developed Nusselt number value of 7.9 predicted using the correlation of Meyer and Everts [10].

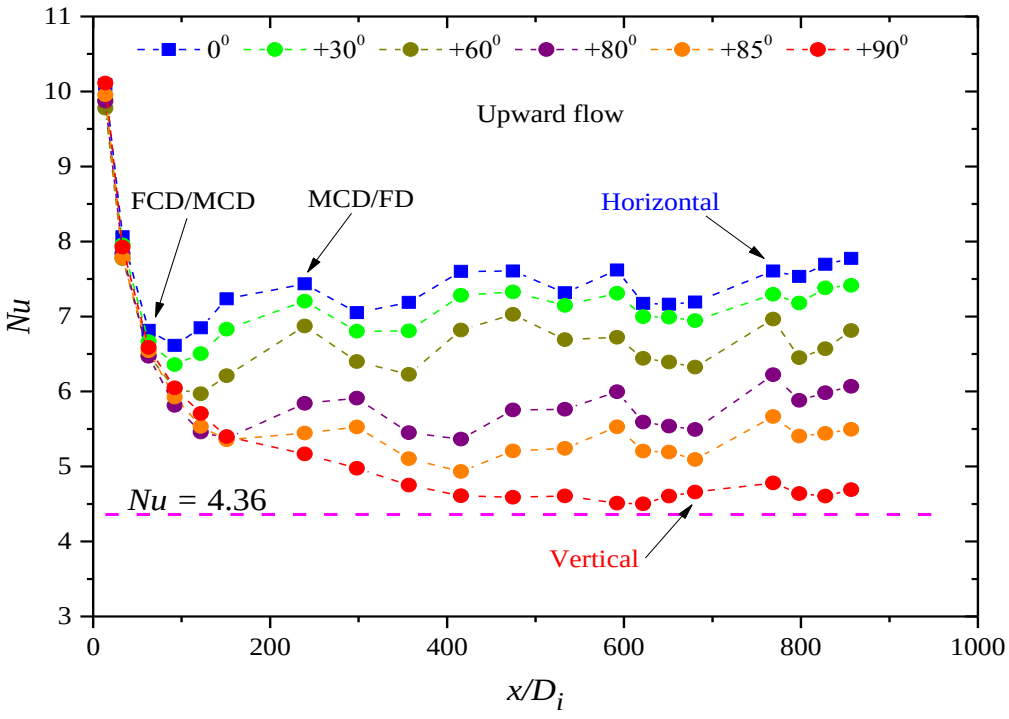

(a)

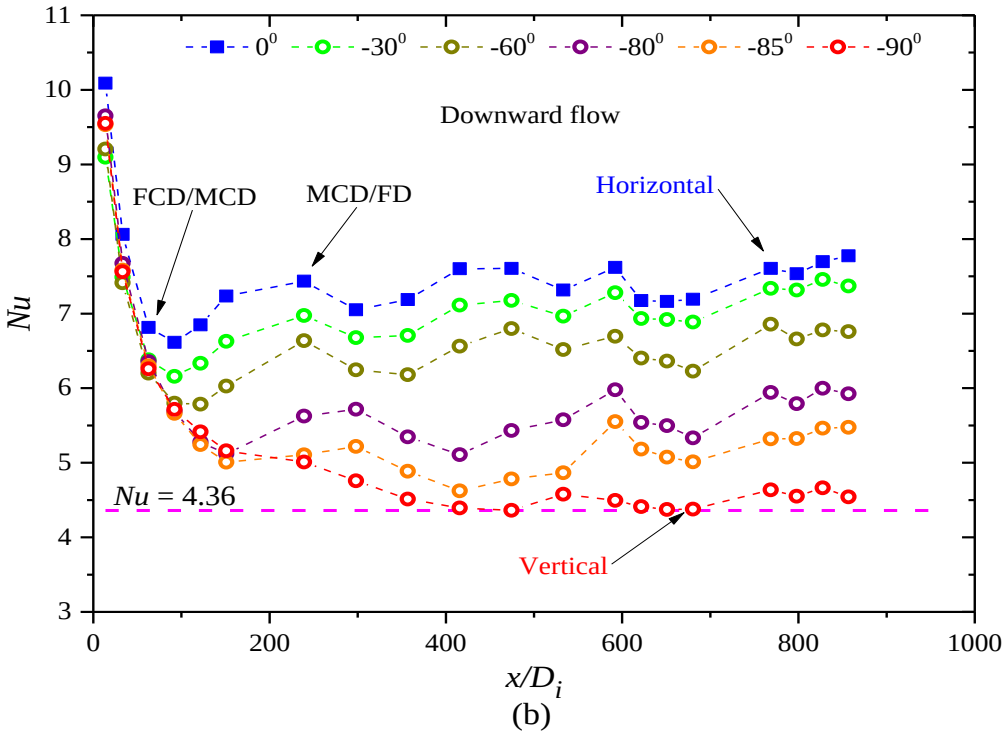

(b)

Fig. 11: Comparison of the local laminar Nusselt numbers as a function of axial position for different inclination angles at a bulk Reynolds number of approximately 1 600 and a heat flux of 6 kW/m^2 for (a) upward flow and (b) downward flow.

(iii) The Nusselt numbers for vertical upward flow (θ = +90°) and vertical downward flow (θ = -90°) converged to the same theoretical forced convection value of 4.36. The Nusselt numbers for vertical upward and downward flow were within 5.7% and 5.3% respectively, of 4.36. Therefore, for downward flow the value was slightly closer to 4.36 than for upward flow.

(iv) Similar to the friction factors in Fig. 9 the Nusselt numbers decreased with increasing inclination angle. The Nusselt number enhancement for the other inclination angles compared with vertical flow could therefore only be because of mixed convection.

(v) The three regions (Forced Convection Developing (FCD) , Mixed Convection Developing (MCD) and Fully Developed(FD)) which were recently defined by Meyer and Everts [10] for mixed convective laminar flow, were also observed in Fig. 11 based on the different inclination angles. For horizontal flow, the laminar Nusselt numbers decreased along the tube length up to x/D_i = 63. Between x/D_i = 63 and x/D_i = 239, buoyancy effects became significant which caused the Nusselt numbers to increase along the tube length due to the increasing thermal boundary layer thickness [10]. The Nusselt numbers became approximately constant after x/D_i = 239, which indicated that the flow was fully developed. The FCD/MCD boundary occurred at x/D_i = 63 for horizontal flow, but was delayed to x/D_i = 92, x/D_i = 122 and x/D_i = 151 as the inclination angle was increased to 30°, 60° and 80° respectively. This is as expected, because Meyer and Everts [10] found that the FCD/MCD boundary occurred earlier (in terms of axial position) with increasing buoyancy effects and it is known from Fig. 9 and Fig. 11 that buoyancy effects decreased with increasing inclination angles. The axial position of the MCD/FD boundary also increased with increasing inclination angles, which confirmed that buoyancy effects decreased the thermal entrance length [10]. Furthermore, as indicated by Meyer and Everts [10], buoyancy effects caused the Nusselt numbers in the MCD and FD regions to increase, which explains why the laminar Nusselt numbers in Fig. 11 decreased with increasing inclination angle.

(vi) The Nusselt number results were symmetric around the inclination angle of 0°. Thus, the results of -30° and +30°, -45° and +45° (not shown here), -60° and +60°, -85° and +85°, etc. were all the same. These same symmetry conclusions were made for the friction factors in Fig. 9.

To prove the symmetry around the inclination angle of 0°, Fig. 12 compares the average fully developed Nusselt numbers as a function of inclination angles at approximately the same bulk fully developed Reynolds numbers (for instance at a Reynolds number of approximately 1 600, the bulk Reynolds number at $\theta = 0°$ was 1 610 and at $\theta = -90°$ was 1 580). This figure indicates that in general the Nusselt numbers increased with decreasing $|\theta|$ due to the increased buoyancy effects. At a 30° increment from the vertical orientation (i.e. from 90° to 60°) the Nusselt numbers at a Reynolds number of 1 600 increased by 44%, while for a 30° increment from 30° to 0°, the increase was only 4%. Therefore, similar to the diabatic friction factors in Fig. 9, small changes in inclination angle near vertical flows led to significant changes in the buoyancy effects.

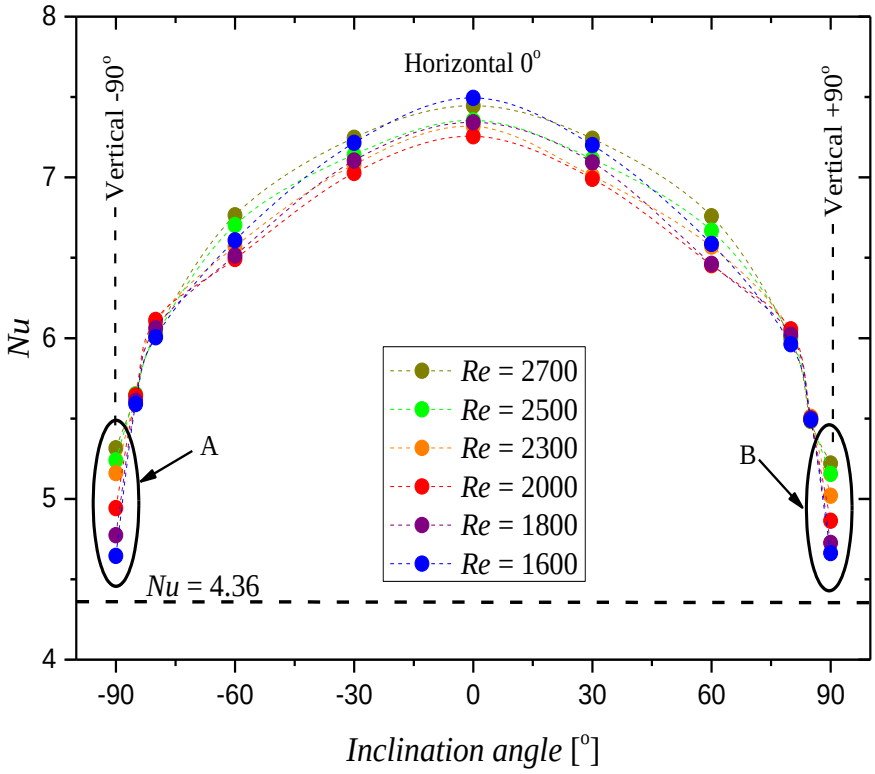

Fig. 12: Average Nusselt numbers as a function of inclination angle for fully developed laminar flow at different bulk Reynolds numbers and a heat flux of 6 kW/m^2.

To clarify the decreasing buoyancy effects with increasing inclination angle, the free body diagrams showing the components of buoyancy forces acting on the fluid flow for different tube orientations are given in Fig. 13. For horizontal flow (Fig. 13(a)), the buoyancy forces act perpendicular to the flow axis and therefore create the maximum disturbances within the flow, in the form of secondary flow [73]. This distorts the thermal boundary layer by decreasing its

thickness and thereby enhancing the heat transfer. As indicated in Fig. 13(d), the buoyancy force, F_b, is a maximum when the tube is in a horizontal orientation as $\cos\theta = 1$ for $\theta = 0°$. At inclined angles (Fig. 13(b)) the magnitude of the buoyancy force ($F_b \cos\theta$) decreases with $\cos\theta$ and reaches a minimum for vertical upward and downward flow (Fig. 13(c)). For vertical flow, the inertia forces dominate the buoyancy forces. A similar behaviour was also observed by Tian et al. [23] in a narrow rectangular channel where mixed convection was induced at different inclination angles (near vertical inclinations between 60° to 90°). For each Reynolds number of the vertical inclinations (±90°), identified as A and B in Fig. 12, the Nusselt number increased as function of Reynolds number. This increase was more significant for vertical flow than at other inclination angles. According to Bashir et al. [72], for Reynolds number higher than approximately 1 000, the laminar heat transfer coefficients in vertical tubes were a function of Reynolds number and independent of flow direction, buoyancy and heat flux.

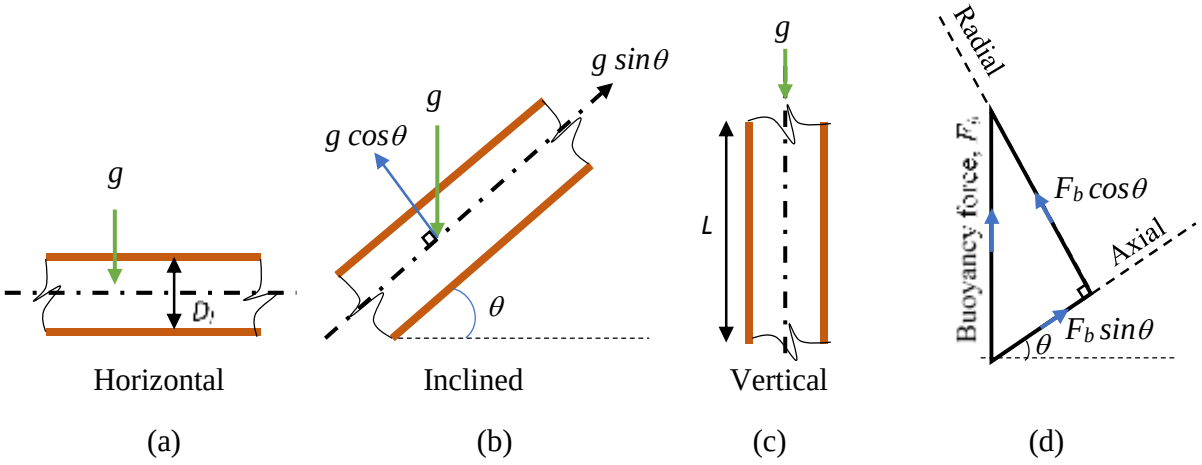

Fig. 13: Components of the buoyancy force for different tube orientations.

6.1.4 Laminar Nusselt number and friction factor correlations

A mixed convection Nusselt number correlation can be expressed as the sum of a forced convection part, Nu_{FC}, plus a mixed convection part, Nu_{MC}, that enhances the heat transfer:

$$Nu = Nu_{FC}(Re) + Nu_{MC}(Pr, Gr, Re) \tag{21}$$

The recently developed forced convection Nusselt number correlation of Bashir et al. [72] was used for the forced convection part:

$$Nu_{FC} = 4.36 + 5.36 \times 10^{-9}\, Re^{2.39} \tag{22}$$

For Reynolds numbers lower than 1 000, the Nusselt numbers converged to a value of 4.36. For higher Reynolds numbers the Nusselt number increased with Reynolds number.

To find an appropriate correction for the mixed convection part, more experiments were conducted at finer inclination angle increments near vertical upward and downward flow, because more changes were observed at these angles. Fig. 14 compares the fully developed Nusselt numbers at a Reynolds number of 1 600 for different inclination angles with a cosine curve. This figure indicates that the expected correction of $cos\theta$ (that is $Nu(\theta) = Nu_{FC} + (Nu - Nu_{FC})cos\theta$) to account for mixed convection heat transfer is insufficient, especially for $60° < \theta < 89°$ (as well as $-60° < \theta < -89°$).

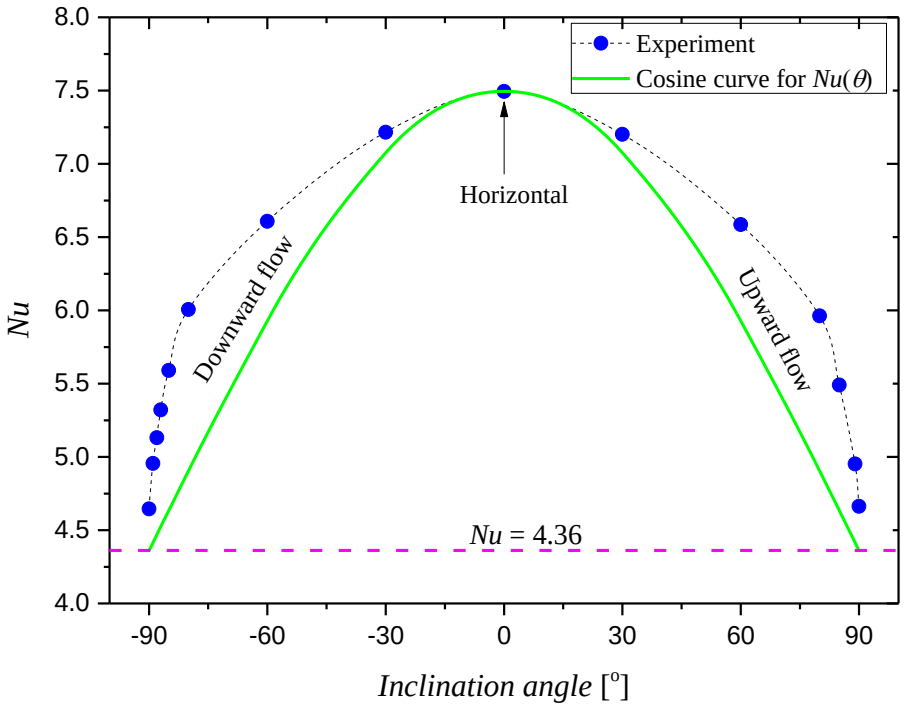

Fig. 14: Average fully developed laminar Nusselt numbers as a function inclination angle for a bulk Reynolds number of 1 600 and a heat flux of 6 kW/m^2.

For horizontal flow, the buoyancy forces, F_b, acted perpendicular to the flow direction and $gcos\theta = g$ when $\theta = 0°$, while for vertical flow it acted parallel to the flow and $gcos\theta = 0$ when $\theta = \pm 90°$. Therefore, a $gcos\theta$ correction gave the correct answers for vertical and horizontal flow. As indicated in Fig. 13, the components of the buoyancy force acted in both the radial and axial directions of the fluid flow for inclined orientations. However, the axial component of the buoyancy force was negligible for vertical upward and downward results, because the Nusselt numbers were approximately equal to the forced convection Nusselt numbers [72]. The horizontal results indicated that the component of the buoyancy force normal to the axis of the fluid flow was the main contributing factor for the heat transfer enhancement and should therefore be used in quantifying the buoyancy effect on heat transfer for inclined tubes.

Because the inclination angle influenced the buoyancy forces, it was decided to correct the Grashof numbers and modified Grashof numbers, which is the ratio of buoyancy forces, F_b, to viscous forces, in Eqs. (15) and (16) as follows:

$$Gr_\theta = Grcos\theta \tag{23}$$

and

$$Gr_\theta^* = Gr^* cos\theta \tag{24}$$

The corresponding Rayleigh numbers were thus:

$$Ra_\theta = Gr_\theta Pr \tag{25}$$

and

$$Ra_\theta^* = Gr_\theta^* Pr \tag{26}$$

This is similar to the approach followed by Rolle [74], who defined an "inclined plane Grashof number" for free convection from a flat plate. In our case, we similarly referred to it as the "inclined tube Grashof number" or "inclined tube Rayleigh number".

The Nusselt number enhancement due to inclination angle was a function of *Pr*, *Re* and Gr_θ or Gr_θ* and could therefore be accounted for by making use of the Reynolds number and inclined tube Rayleigh number:

$$Nu_{MC} = 0.053\left(\frac{Ra_\theta{}^{0.2}}{Re^{0.1}}\right)^{2.9} \tag{27}$$

or in terms of the modified Rayleigh number:

$$Nu_{MC} = 0.032\left(\frac{Ra_\theta^{*\,0.15}}{Re^{0.08}}\right)^{3.48} \tag{28}$$

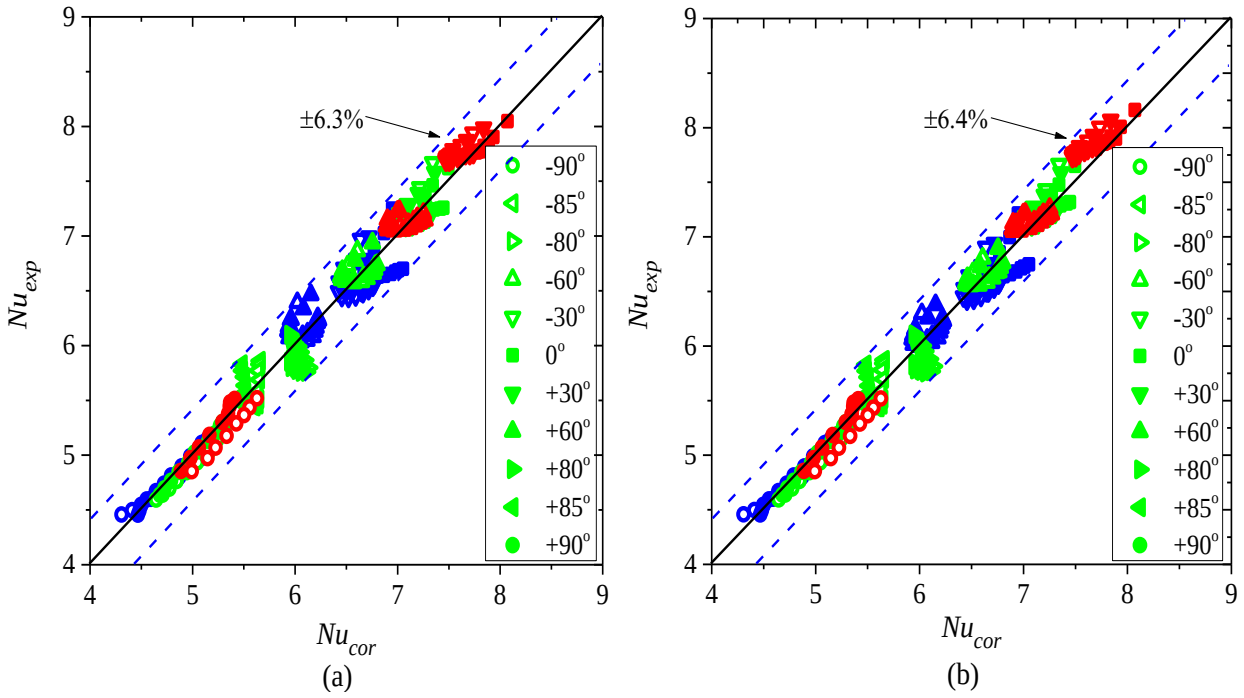

Fig. 15: Comparison of the average laminar Nusselt number correlation Eq. (21) for fully developed flow with experimental results for the different inclination angles and heat fluxes using Eq. (22) and (a) Eq. (27) and (b) Eq. (28). The blue, green and red markers represent heat fluxes of 4 kW/m^2, 6 kW/m^2, and 8 kW/m^2, respectively.

When using constant heat fluxes, the use of Eq. (28) is more convenient [10, 12, 34, 38], because the temperature differences used to determine the Grashof numbers and thus Rayleigh numbers in Eq. (27) are normally not known while the heat fluxes are.

Eq. (21) (with Eqs. (22), (27) and (28)) were valid for $-90° \leq \theta \leq 90°$, $593 \leq Gr_\theta \leq 18\,040$, $3\,346 \leq Gr_\theta^* \leq 146\,014$, $1\,000 \leq Re \leq 3\,500$ and $3 \leq Pr \leq 7$. For $600 \leq Re \leq 1\,000$ and $\theta = \pm 90°$ [72], $Ra_\theta^* = 0$, and thus, $Nu_{MC} = 0$. With our experimental set-up we could not conduct

experiments at lower Reynolds numbers than approximately 600, because the outlet temperatures became too large.

Fig. 15 compares the experimental Nusselt numbers at different heat fluxes and inclination angles with the calculated values (Nu_{cor}) from Eq. (21) with Eq. (27) in Fig. 15(a) and with Eq. (28) in Fig. 15(b). In Fig. 15(a), where the Grashof numbers were determined from the measured temperature differences, the maximum deviation was 6.3% and the average deviation was 1.8%. In Fig. 15(b), where the Grashof numbers were determined from the measured heat fluxes, the maximum deviation was 6.4% and the average deviation was 1.7%.

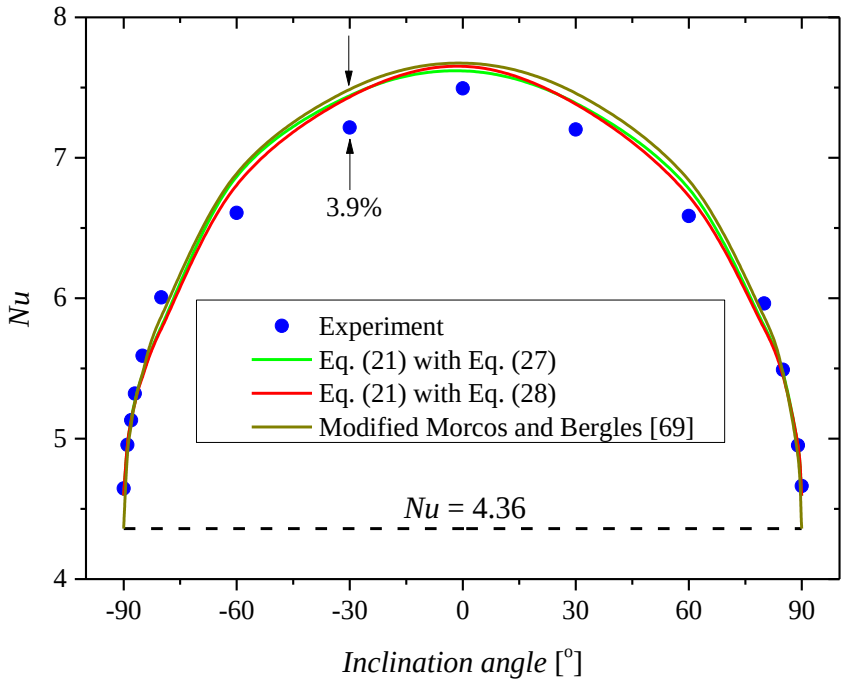

Fig. 16: Comparison of laminar fully developed Nusselt number correlations, Eq. (21) (with Eq. (27) and Eq. (28)) with the experimental data at a bulk Reynolds number of approximately 1 600 and a heat flux of 6 kW/m^2 for different inclination angles.

Fig. 16 compares the fully developed Nusselt numbers at a bulk Reynolds number of approximately 1 600 and a heat flux 6 kW/m^2 for different inclination angles with the Nusselt numbers predicted using Eq. (21) (with Eq. (27) and Eq. (28)). The average deviation was 1.8% and the maximum difference was 3.9%. The inclined Grashof numbers (Eqs. (23) and (24)) were also used in the mixed convection laminar flow correlation of Morcos and Bergles [69] and the

average deviation between the Nusselt numbers predicted using Eq. (21) with Eq. (28) and the correlation of Morcos and Bergles [69] was 2.8%. A maximum deviation of 20% was found for vertical flows (forced convection) because their correlation did not account for variable property forced convection Nusselt numbers which changed with Reynolds number. The inclined tube modified Grashof number, Gr_θ* was evaluated at the film temperature.

For the fully developed isothermal friction factors, Fig. 7 indicated that the friction factors were approximately equal to the Poiseuille correlation of 64/*Re* for all inclination angles. Similar to the approach used by Tam and Ghajar [11] and Tam et al. [54] for the diabatic friction factors, the isothermal friction factors were multiplied with the bulk-to-wall-viscosity ratios, (μ_b/μ_w), as a function of the inclined tube Grashof and Prandtl numbers:

$$f = \left(\frac{64}{Re}\right)\left(\frac{\mu_b}{\mu_w}\right)^{0.0016 Gr_\theta^{0.67} Pr^{0.011}} \tag{29}$$

and in terms of modified inclined Grashof numbers:

$$f = \left(\frac{64}{Re}\right)\left(\frac{\mu_b}{\mu_w}\right)^{0.0016 Gr_\theta^{*0.56} Pr^{0.011}} \tag{30}$$

Eqs. (29) and (30) were valid for $-90° \le \theta \le 90°$, $593 \le Gr_\theta \le 18\,040$, $3\,346 \le Gr_\theta^* \le 146\,014$, $1.04 \le \mu_b/\mu_w \le 1.25$, $1\,000 \le Re \le 3\,500$ and $3 \le Pr \le 7$. For $600 \le Re \le 1\,000$ and $\theta = \pm 90°$, the friction factors were not a function of Grashof number and were considered as forced convection friction factors; thus $f = 64/Re$ [72].

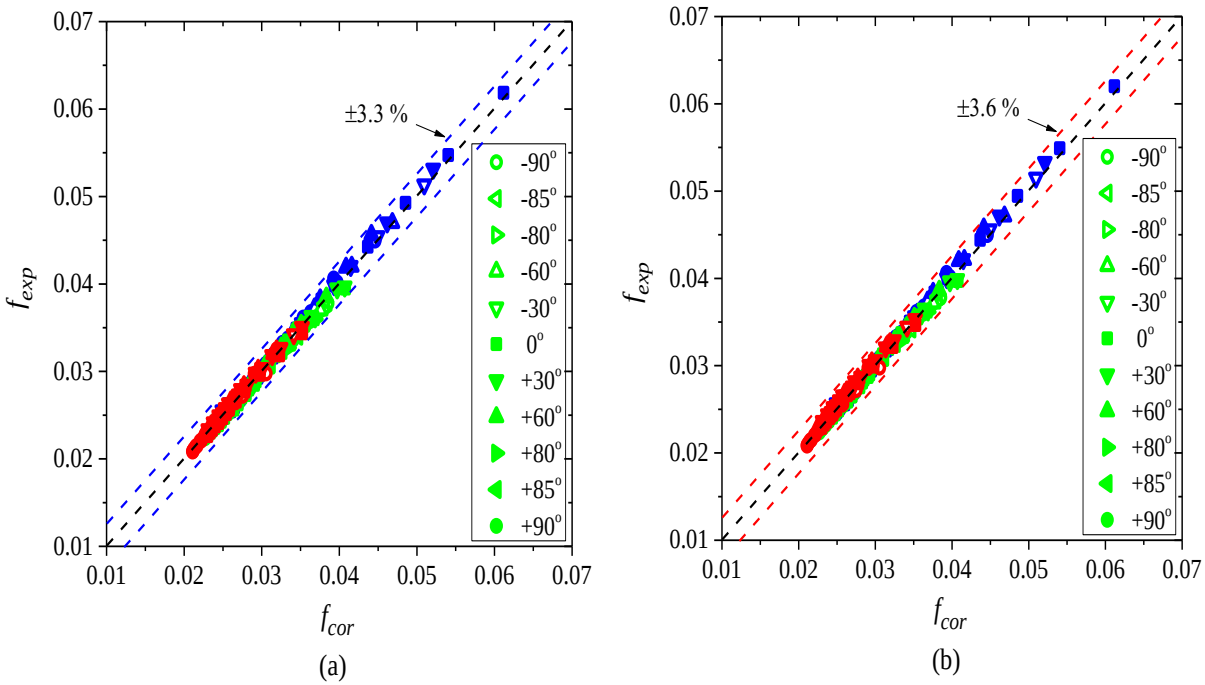

Fig. 17: Comparison of the laminar fully developed diabatic friction factor correlations with the experimental results for the different inclination angles at different heat fluxes using (a) Eq. (29) and (b) Eq. (30). The blue, green and red markers represent heat fluxes of 4 kW/m^2, 6 kW/m^2, and 8 kW/m^2, respectively.

The experimental friction factors different heat fluxes and inclination angles were compared to the calculated values from Eq. (29) in Fig. 17(a) and with Eq. (30) in Fig. 17(b). In Fig. 17(a), where the Grashof numbers were determined from the measured temperature differences, the maximum deviation was 3.3% and the average deviation was 1%. In Fig. 17(b), where the Grashof numbers were determined from the measured heat fluxes, the maximum deviation was 3.6% and the average deviation was 1%.

6.1.5 Transitional flow

Fig. 18 compares the average fully developed Colburn *j*-factors at a heat flux of 6 kW/m^2 for different inclination angles as a function of the bulk fully developed Reynolds number. As there were no significant difference in the results for upward and downward flow (Fig. 12), only results for upward flow were given.

In the laminar flow regime, the Colburn *j*-factors decreased with increasing Reynolds numbers, as expected. Furthermore, at a fixed Reynolds number, the laminar Colburn *j*-factors decreased with increasing inclination angle from horizontal to vertical flow.

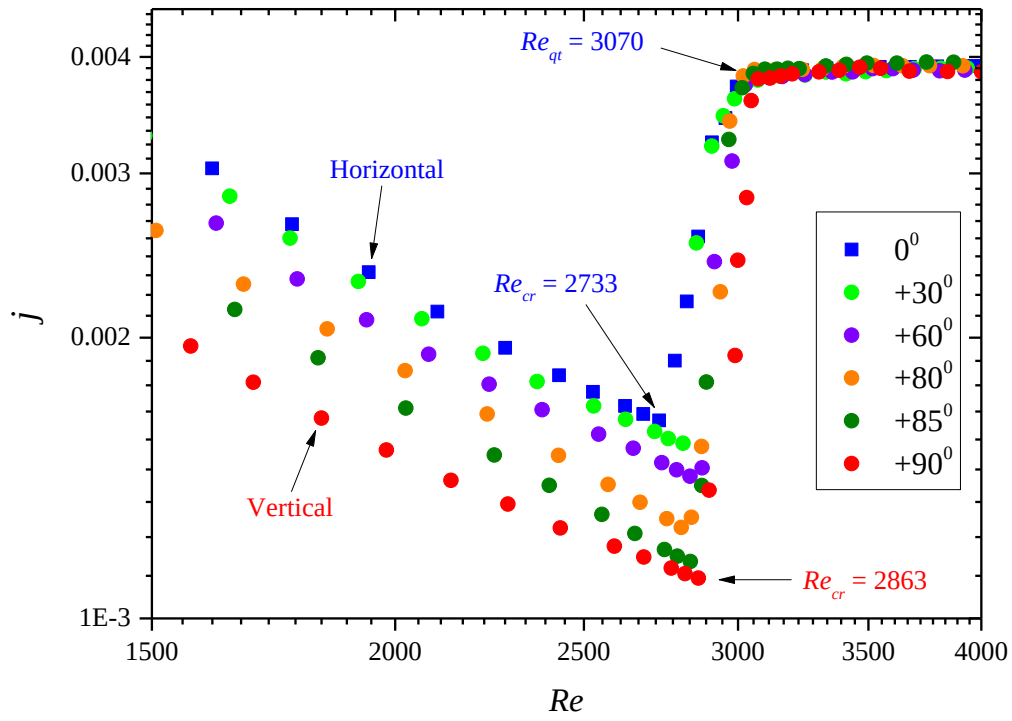

Fig. 18: Comparison of the average fully developed Colburn *j*-factors as a function of Reynolds number for upward flow at different inclination angles at constant heat flux of 6 kW/m^2.

The critical Reynolds number (Re_{cr}) at which transition started, as defined by Everts and Meyer [12], corresponded to the point where the gradient of the laminar Colburn *j*-factor changed from a negative to a positive gradient. Fig. 18 indicates that for horizontal flow (θ = 0°), the critical Reynolds number was 2 733. Transition ended (Re_{qt}) for horizontal flow at a Reynolds number of approximately 3 070, where the flow entered the quasi-turbulent flow regime. Fig. 18 also indicates that the critical Reynolds numbers increased with increasing inclination angle from 2 733 for horizontal flow to 2 863 for vertical flow. Everts and Meyer [12] found that buoyancy effects caused transition to occur earlier. Hence, as the buoyancy effects decreased due to increasing inclination angles, the start of transition was delayed.

To investigate the Colburn *j*-factors in the transitional flow regime, Fig. 19 compares the Colburn *j*-factors at the start, j_{cr}, and end, j_{qt}, of the transitional flow regime as a function of inclination angle. As expected, the maximum Colburn *j*-factor at the start of transition occurred at the horizontal orientation (0°), where buoyancy forces were at its maximum, and decreased as the

inclination angle increased in the upward and downward flow directions. However, the Colburn *j*-factors at the end of transition remained constant at 0.00389, which confirmed that the heat transfer coefficients at the end of the transitional flow regime was independent of inclination angle (or Grashof number). The effect of buoyancy decreased with increasing Reynolds number in the transitional flow regime because of the increase in mass flow rates (inertia forces) that enhanced mixing (turbulence) and dominated buoyancy effects. At a quasi-turbulent Reynolds number of 3 500, all 11 Colburn *j*-factor values of the different inclination angles were within 0.1% of the average value of 0.00389. The turbulent flow regime, (not shown in Fig. 18) was similar to the quasi-turbulent flow regime in which the inertia forces were much higher than the buoyancy forces. The results were therefore Grashof number independent, as was also found by Meyer and Everts [10] and Everts and Meyer [12, 34].

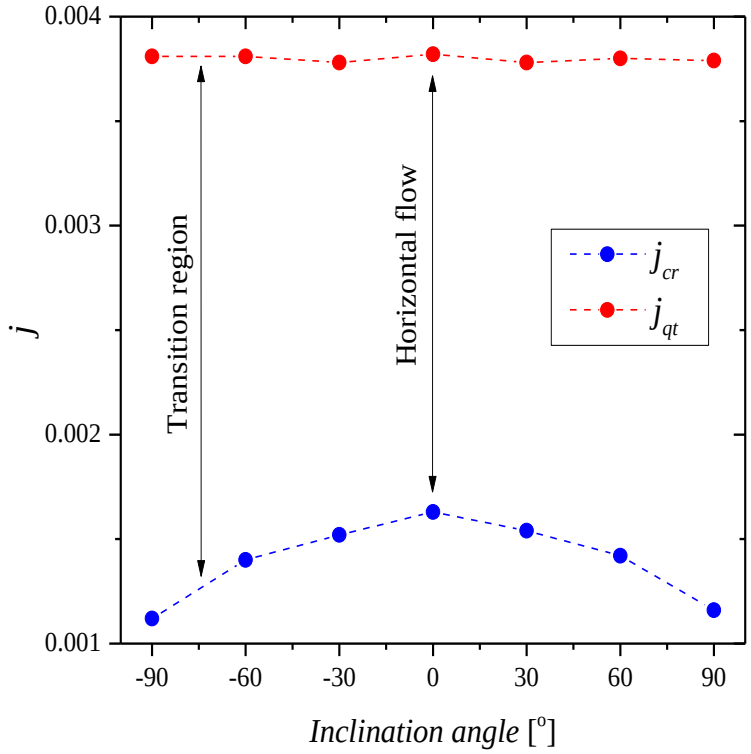

Fig. 19: Comparison of the Colburn *j*-factors at the start, j_{cr}, and end, j_{qt}, of the transitional flow regime as a function of inclination angle at a heat flux of 6 kW/m^2.

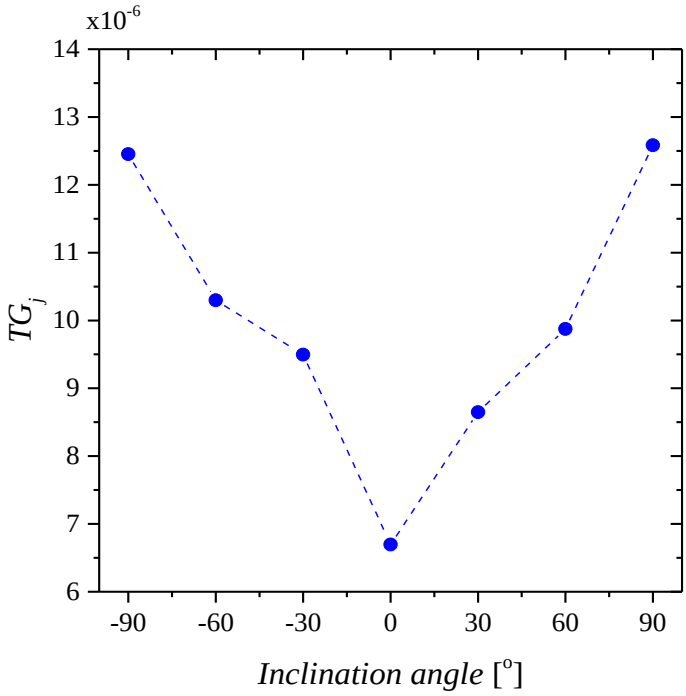

Fig. 20: Comparison of transition gradients of the Colburn *j*-factor (TG_j) as a function of inclination angle at a heat flux of 6 kW/m^2.

Fig. 20 compares the transition gradients (Eq. (19) as defined by Everts and Meyer [12]) as a function of inclination angle. This figure indicates that the transition gradient increased from horizontal to vertical flow. This was because the critical Reynolds numbers increased with inclination (due to decreasing buoyancy effects) while the end of transition Reynolds number remained relatively constant (Fig. 21). A similar trend was also found in the transition gradients of the friction factors, where it increased with an increase in the inclination angle from horizontal to vertical flow.

To investigate the effects of flow direction and buoyancy on the boundaries of the transitional flow regime, Fig. 21 compares the Reynolds numbers at which transition started and ended as a function of inclination angle in the upward and downward flow directions at a heat flux of 6 kW/m^2. It should be noted (taken into consideration the uncertainties) that this graph which was generated from the Colburn *j*-factors results, compares very well with Fig. 10 which was generated from the friction factor results. The good agreement can be expected, because Everts and Meyer [34] recently showed that there is a direct relationship between heat transfer and pressure drop in the transitional flow regime.

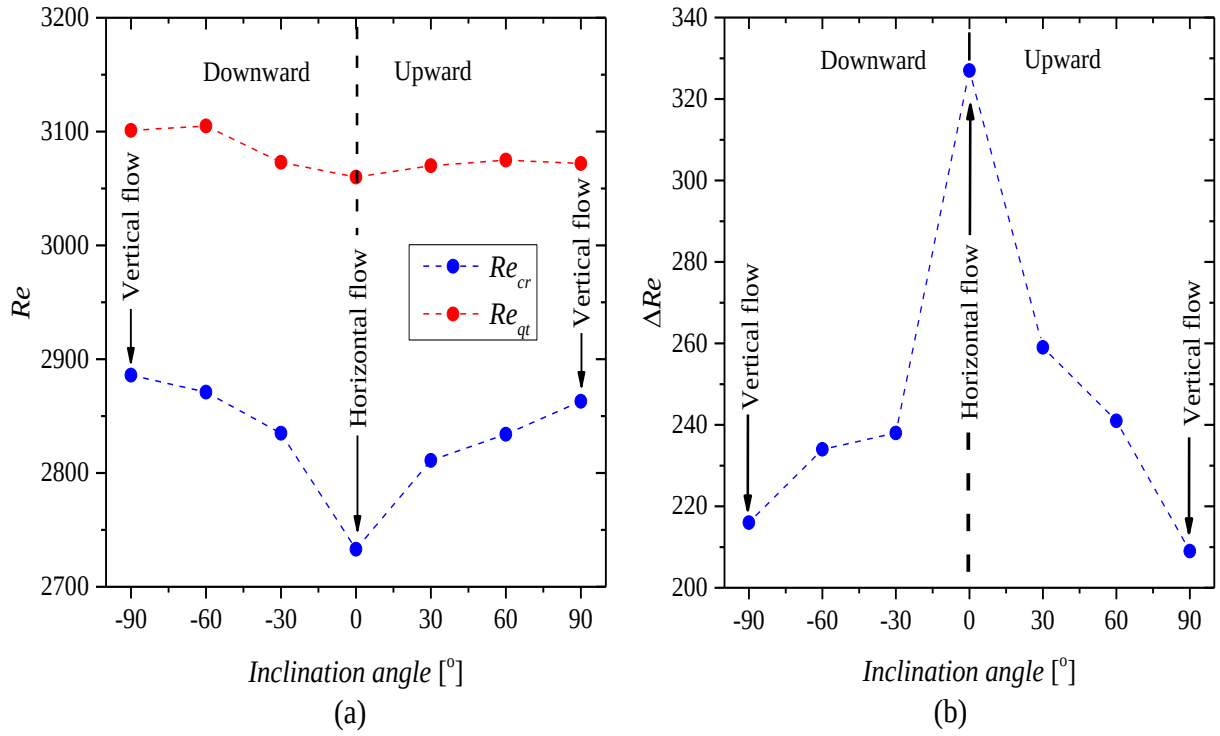

Fig. 21: Comparison of (a) the Reynolds numbers at which transition started and ended and (b) the width of transition as a function of inclination angle at a heat flux of 6 kW/m^2.

When the inclination angle was increased and decreased from the horizontal, (θ = 0°) to the vertical upward flow (θ = +90°) and vertical downward flow (θ = –90°), the critical Reynolds numbers, Re_{cr}, increased. However, similar to the results in Fig. 18, the Reynolds numbers, Re_{qt}, at which transition ended remained relatively constant for all the inclination angles. Fig. 21(b) compares the width of the transitional flow regime, ΔRe (Eq. (18)), as a function of inclination angle. This graph indicates that that the width of the transitional flow regime was a maximum for horizontal flow and decreased as the inclination angle increased in the upward and downward flow directions to vertical flow, where buoyancy was insignificant (forced convection condition). Thus, the maximum width of transition was found for horizontal flow where the buoyancy forces were the largest.

6.1.6 Schematic summary

Because the important transition values at different inclination angles were challenging to identify from the experiments, the heat transfer and pressure drop results are summarized

schematically in Fig. 22(a) and (b) respectively, as a function of Reynolds number. The blue, orange, green and red curves represent the horizontal $\theta = 0°$, ±30°, ±60° and vertical ±90°, inclinations.

In the laminar flow regime (Fig. 22(a)), the Nusselt numbers for vertical flow converged to the forced convection Nusselt number of 4.36. At a fixed Reynolds number, the Nusselt numbers increased with decreasing inclination angle from vertical upward or downward ($\theta = \pm 90°$) to horizontal ($\theta = 0°$) flow, due to the increase in the inclined tube Grashof number (buoyancy). Our experimental data also indicated that the Prandtl numbers during this process increased (especially near the wall) which contributed towards increased Rayleigh numbers (product of the Grashof and Prandtl numbers). A significant increase in Nusselt number occurred as buoyancy effects became significant when the inclination angle was changed with 30° from vertical (±90°) downward or upward $\theta = \pm 60°$. A similar increase of 30° from horizontal flow ($\theta = 0°$) caused a relatively small change in the Nusselt number. The reason is that the buoyance already occurred when the tube was in a horizontal orientation and the 30° change in inclination angle just slightly decreased the inclined tube Grashof number (buoyancy).

A similar behaviour was observed with the laminar fully developed diabatic friction factors in (Fig. 22(b)) where the friction factors a fixed Reynolds number increased as the inclination angle decreased from vertical upwards or downwards flow ($\theta = \pm 90°$) to horizontal flow ($\theta = 0°$) flow. The friction factors for vertical flow converged to the forced convection and isothermal friction factors of 64/*Re*.

As indicated by points A to D in Fig. 22, the critical Reynolds numbers, Re_{cr}, increased as the inclination angle increased from horizontal to vertical. However, the Reynolds numbers at which transition ended, Re_{qt}, remained relatively constant (at point X) for all the inclination angles. As the Grashof number decreased due to increased inclination angle, the width of the transitional flow regime decreased. Furthermore, dotted line A-X (horizontal flow) and dotted line D-X (vertical flow) indicate that the transition gradients of the Nusselt numbers (TG_{Nu}) in (Fig. 22(a)) and that of the friction factors (TG_f) in (Fig. 22(b)) increased with increasing inclination angle.

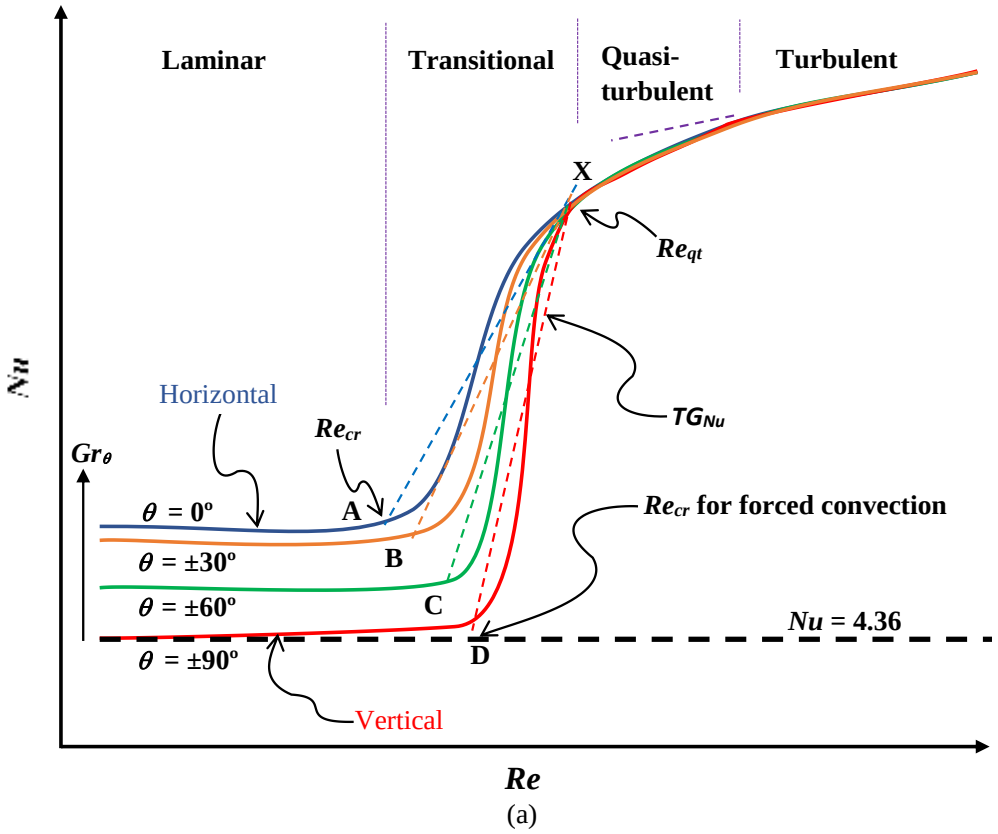

(a)

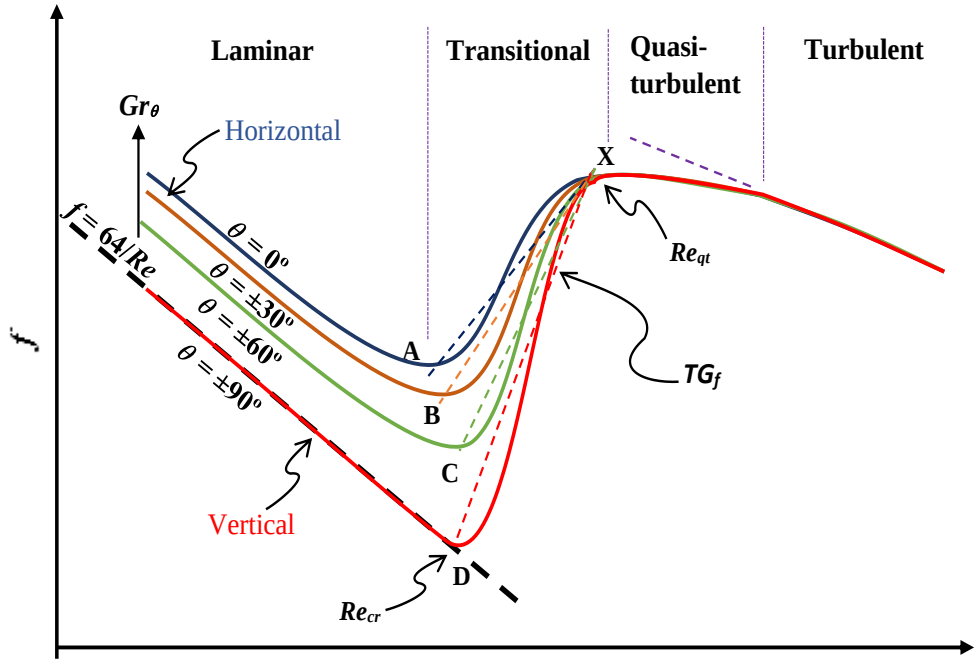

(b)

Fig. 22: Schematic representation of (a) the Nusselt number and (b) the friction factor, as a function of Reynolds number for upward and downward flow at different inclination angles and constant heat flux.

In the quasi-turbulent flow regime, inclination had a negligible effect on the heat transfer and pressure drop results, because the turbulent motion of the fluid completely suppressed the buoyancy effects. The turbulent flow regime is expected to be similar to the quasi-turbulent flow regime.

Developing flow heat transfer for horizontal and vertical flow

Fig. 23 compares the heat transfer results for developing and fully developed flow at horizontal (0°) and vertical upward (+90°) inclinations as function of local Reynolds number. Only the vertical upward flow results have been included, because Fig. 12 indicated that there was no significant difference in the results of upward and downward flows. In the laminar flow regime, the green line represents the Nusselt number of 4.36 for fully developed forced convection heat transfer, while the orange line represents the correlation of Meyer and Everts [10] for developing and fully developed mixed convection heat transfer. Furthermore, points A-H in Fig. 23 corresponds to points A-H in Fig. 24.

Fig. 23(a) indicates that near the inlet of the test section (at $x/D_i = 33$), the laminar Colburn *j*-factors were higher than the fully developed line for forced convection conditions ($Nu = 4.36$). There was no difference between the results for horizontal and vertical flows, because buoyancy effects were suppressed by the thin boundary layers and the results fell into the Forced Convection Developing (FCD) region as defined by Meyer and Everts [10]. Although a similar trend was observed in Fig. 23(b), the Colburn *j*-factors were less than in Fig. 23(a) because the heat transfer coefficients decreased along the tube length as the flow developed [10].

As the flow continued downstream to $x/D_i = 151$ (Fig. 23(c)), the Colburn *j*-factors for horizontal flow corresponded very well to the correlation of Meyer and Everts [10]. However, the Colburn *j*-factors for vertical flow were less than for horizontal flow, because the buoyancy effects were negligible, while it became significant for horizontal flow. The Colburn *j*-factors remained higher than the theoretical forced convection Nusselt number of 4.36 which indicated that the flow was still developing.

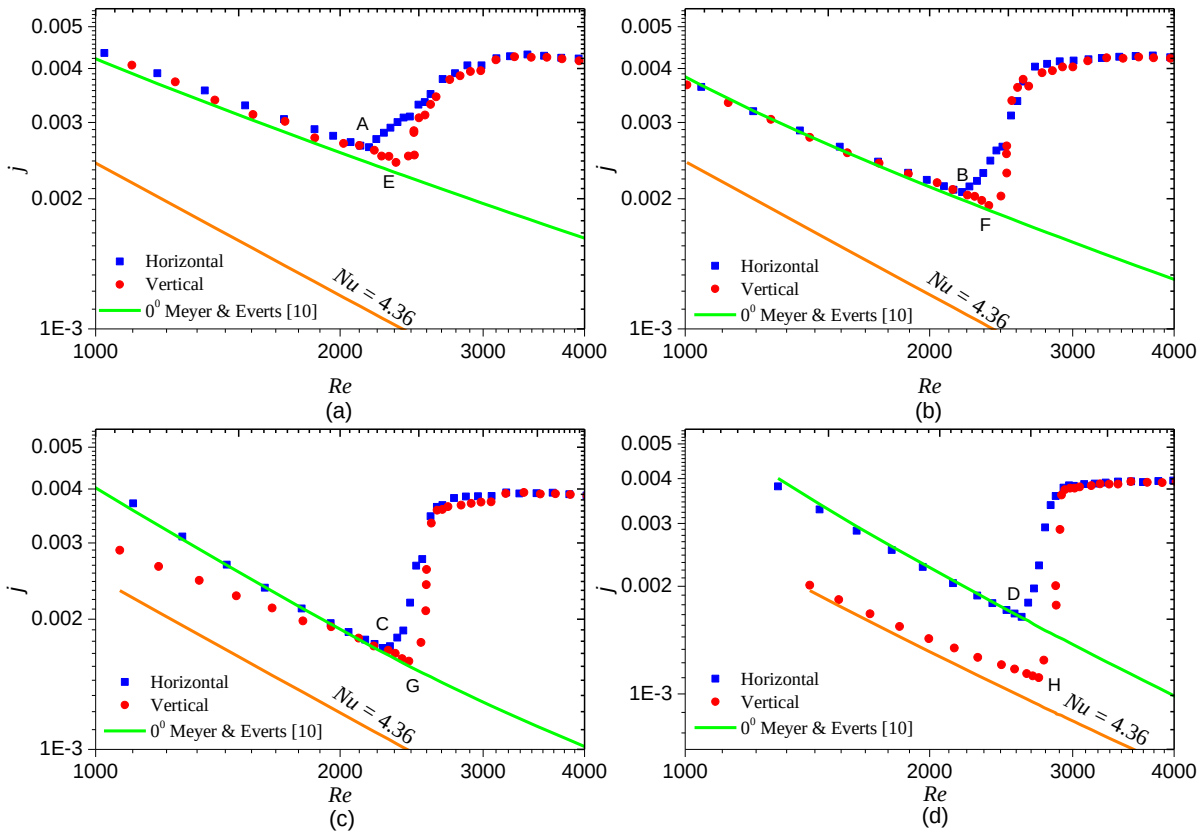

Fig. 23: Comparison of local developing and fully developed Colburn *j*-factors as function of (a) x/D_i = 33, (b) x/D_i = 63, (c) x/D_i = 151 and (d) x/D_i = 592, as a function of local Reynolds numbers for horizontal and vertical flow at a heat flux of 6 kW/m^2.

Fig. 23(d) indicates that at x/D_i = 592, the Colburn *j*-factors for vertical flow corresponded well (average deviation of 9%) with the forced convection Nusselt number of 4.36, especially for Reynolds numbers less than 2 000. Furthermore, the Colburn *j*-factors for horizontal flow were significantly higher than for vertical flow, because buoyancy effects enhanced the heat transfer inside the test section.

Fig. 23 also indicates that the start of transition was delayed for vertical flow compared to horizontal flow along the entire tube length. The end of transition occurred at approximately the same Reynolds number for both horizontal and vertical flow. Fig. 24 compares the Reynolds numbers at which transition started in Fig. 23 for horizontal (points A - D) and vertical (points E - H) as a function of axial position. Similar to the horizontal flow results of Everts and Meyer [12] and vertical flow results of Bashir et al. [72], the critical Reynolds numbers increased along the tube length for both horizontal and vertical flows. This was only due to the variation of viscosity

with temperature and transition actually occurred at the same mass flow rate in the entire test section [12]. The increased critical Reynolds numbers of vertical flow compared with horizontal flow was as expected because Everts and Meyer [12] found that buoyancy effects caused transition to occur earlier and buoyancy effects were significant for horizontal flow but negligible for vertical flow (Fig. 23).

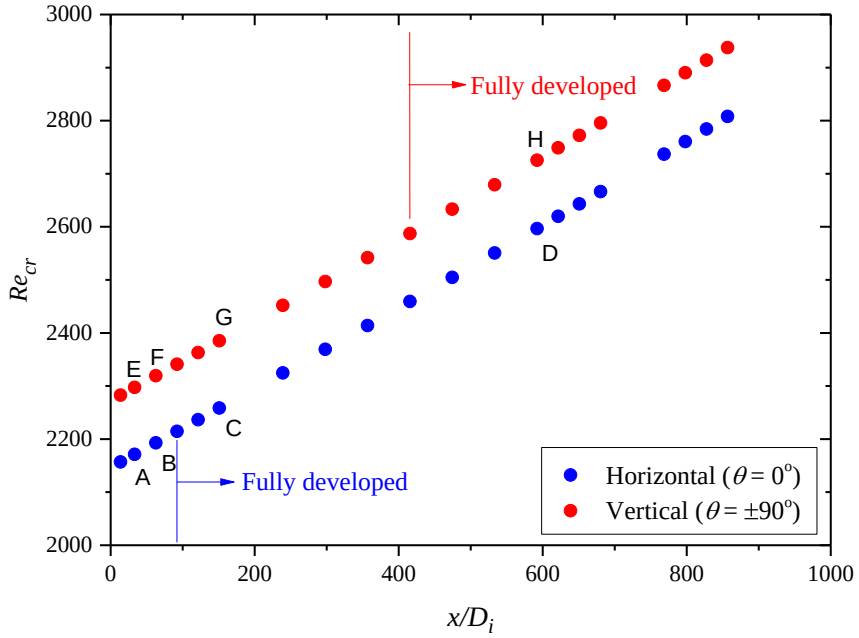

Fig. 24: Comparison of the start of the transition local critical Reynolds numbers as a function of axial location of the tube for developing and fully developed flows of horizontal and vertical inclinations in Fig. 23.

7. Conclusions

The heat transfer and pressure drop of a single-phase mixed convective flow in the laminar and transitional flow regimes in smooth inclined tubes heated at a constant heat flux were experimentally investigated. Experiments were conducted at various inclination angles from vertical upward flow to vertical downward flow, with horizontal flow and several other angles in between. Tests were conducted with water at several heat fluxes from 4 to 8 kW/m^2 and the Reynolds number range covered were from 1 000 to 6 000.

To account for effect of inclination angle on the laminar Nusselt numbers and the friction factors, a simple *inclined tube Grashof/Rayleigh number* was defined. The laminar heat transfer

was expressed as a forced convection part plus an additional enhancement part caused by possible free/mixed convection. Similarly, the laminar flow friction factors were expressed as the forced convection part multiplied by the enhancement part. Fully developed average laminar Nusselt number and friction factor correlations for inclined tubes were developed as a function of the inclined tube Grashof/Rayleigh numbers.

Buoyancy effects were found to be negligible for vertical upward and downward flow and both the heat transfer and pressure drop results were dominated by forced convection only. It was also found that the influences of buoyancy near vertical inclinations was stronger than near horizontal inclinations which caused the laminar heat transfer and pressure drop to increase rapidly near vertical inclinations.

Both the heat transfer and pressure drop results indicated that the Reynolds number at which transition started in the fully developed region increased as the inclination angle increased from horizontal to vertical flow, while the end of transition remained relatively constant for all the inclination angles. This caused the width of the transitional flow regime to decrease as the inclination angle increased. Furthermore, inclination of the test section decreased the buoyancy effects (inclined tube Grashof number) and increased the transition gradient. Because buoyancy had a negligible effect on the quasi-turbulent flow regime, the results were independent of inclination angle. Furthermore, flow directions (upward and downward flows) had negligible influence on the heat transfer coefficients and friction factors. Overall it was concluded that inclination of heated tubes changes the way buoyancy forces acted on the fluid flow and changed the magnitude of the Grashof numbers and thus, transition Reynolds numbers.

8. Acknowledgements

The authors acknowledges the funding received from the Department of Science and Technology (DST) in South Africa and BUK in Nigeria. This work was conducted by the second author as a PhD student under the supervision of the first (professor) and third (post-doctoral fellow) authors.

REFERENCES

[1] D.R.E. Ewim, J.P. Meyer, S.M.A. Noori Rahim Abadi, Condensation heat transfer coefficients in an inclined smooth tube at low mass fluxes, International Journal of Heat and Mass Transfer, 123 (2018) 455-467.

[2] S.P. Olivier, J.P. Meyer, M. De Paepe, K. De Kerpel, The influence of inclination angle on void fraction and heat transfer during condensation inside a smooth tube, International Journal of Multiphase Flow, 80 (2016) 1-14.
[3] A.O. Adelaja, J. Dirker, J.P. Meyer, Experimental study of the pressure drop during condensation in an inclined smooth tube at different saturation temperatures, International Journal of Heat and Mass Transfer, 105 (2017) 237-251.
[4] J.P. Meyer, J. Dirker, A.O. Adelaja, Condensation heat transfer in smooth inclined tubes for R134a at different saturation temperatures, International Journal of Heat and Mass Transfer, 70 (2014) 515-525.
[5] S. Lips, J.P. Meyer, Experimental study of convective condensation in an inclined smooth tube. Part I: Inclination effect on flow pattern and heat transfer coefficient, International Journal of Heat and Mass Transfer, 55(1) (2012) 395-404.
[6] S. Lips, J.P. Meyer, Experimental study of convective condensation in an inclined smooth tube. Part II: Inclination effect on pressure drops and void fractions, International Journal of Heat and Mass Transfer, 55(1) (2012) 405-412.
[7] S. Lips, J.P. Meyer, Stratified flow model for convective condensation in an inclined tube, International Journal of Heat and Fluid Flow, 36 (2012) 83-91.
[8] S. Lips, J.P. Meyer, Two-phase flow in inclined tubes with specific reference to condensation: A review, International Journal of Multiphase Flow, 37(8) (2011) 845-859.
[9] Y.A. Çengel, A.J. Ghajar, Heat and Mass Transfer: Fundamentals & Applications, 5th ed., Mcgraw Hill, New York, 2015.
[10] J.P. Meyer, M. Everts, Single-phase mixed convection of developing and fully developed flow in smooth horizontal circular tubes in the laminar and transitional flow regimes, International Journal of Heat and Mass Transfer, 117 (2018) 1251-1273.
[11] L.M. Tam, A.J. Ghajar, Effect of inlet geometry and heating on the fully developed friction factor in the transition region of a horizontal tube, Experimental Thermal and Fluid Science, 1777(97) (1997) 52-64.
[12] M. Everts, J.P. Meyer, Heat transfer of developing and fully developed flow in smooth horizontal tubes in the transitional flow regime, International Journal of Heat and Mass Transfer, 117 (2018) 1331-1351.
[13] M. Iqbal, J.W. Stachiewicz, Influence of tube orientation on combined free and forced laminar convection heat transfer, Journal of Heat Transfer, 88(1) (1966) 109-116.
[14] A. Al-Sammarraie, R. Jassem, T. K. Ibrahim, Mixed convection heat transfer in inclined tubes with constant heat flux, European Journal of Scientific Research, 97(1) (2013) 144-158.
[15] H.A. Mohammed, Y.K. Salman, Combined convection heat transfer for thermally developing aiding flow in an inclined circular cylinder with constant heat flux, Applied Thermal Engineering, 27(8) (2007) 1236-1247.
[16] J. Orfi, N. Galanis, C.T. Nguyen, Laminar mixed convection in the entrance region of inclined pipes with high uniform heat fluxes, American Society of Heating, Refrigerating and Air-Conditioning Engineers, Inc., Atlanta, GA (United States), 1998.
[17] G.S. Barozzi, E. Zanchini, M. Mariotti, Experimental investigation of combined forced and free convection in horizontal and inclined tubes, Meccanica, 20(1) (1985) 18-27.
[18] T. Maré, N. Galanis, I. Voicu, J. Miriel, Experimental analysis of mixed convection in inclined tubes, Applied Thermal Engineering, 26(14–15) (2006) 1677-1683.

[19] J. Orfi, N. Galanis, C.T. Nguyen, Laminar fully developed incompressible flow with mixed convection in inclined tubes, International Journal of Numerical Methods for Heat & Fluid Flow, 3(4) (1993) 341-355.
[20] J. Orfi, N. Galanis, C.T. Nguyen, Bifurcation in steady laminar mixed convection flow in uniformly heated inclined tubes, International Journal of Numerical Methods for Heat & Fluid Flow, 9(5) (1999) 543-567.
[21] J. Orfi, N. Galanis, Developing laminar mixed convection with heat and mass transfer in horizontal and vertical tubes, International Journal of Thermal Sciences, 41(4) (2002) 319-331.
[22] D. Choudhury, S.V. Patankar, Combined forced and free laminar convection in the entrance region of an inclined isothermal tube, Journal of Heat Transfer, 110(4) (1988) 901-909.
[23] C. Tian, J. Wang, X. Cao, C. Yan, A.A. Ala, Experimental study on mixed convection in an asymmetrically heated, inclined, narrow, rectangular channel, International Journal of Heat and Mass Transfer, 116 (2018) 1074-1084.
[24] C. Tian, M. Yan, J. Wang, X. Cao, C. Yan, S. Yu, Experimental investigation of flow and heat transfer for natural circulation flow in an inclined narrow rectangular channel, Progress in Nuclear Energy, 98 (2017) 266-276.
[25] G.C. Vliet, Natural convection local heat transfer on constant-heat-flux inclined surfaces, Journal of Heat Transfer, 91(4) (1969) 511-516.
[26] T. Fujii, H. Imura, Natural-convection heat transfer from a plate with arbitrary inclination, International Journal of Heat and Mass Transfer, 15(4) (1972) 755-767.
[27] N. Rani, H. Setia, M. Dutt, R. Wanchoo, Natural convection heat transfer from inclined cylinders: A unified correlation, International Journal of Mathematical, Computational, Physical and Quantum Engineering, 8(1) (2014) 100-105.
[28] P.H. Oosthuizen, D. Naylor, An Introduction to Convective Heat Transfer Analysis, McGraw-Hill, New York, 1999.
[29] A.J. Ghajar, L.M. Tam, Heat transfer measurements and correlations in the transition region for a circular tube with three different inlet configurations, Experimental Thermal and Fluid Science, 8(1) (1994) 79-90.
[30] A.J. Ghajar, L.M. Tam, Laminar-transition-turbulent forced and mixed convective heat transfer correlations for pipe flows with different inlet configurations, American Society of Mechanical Engineers, Heat Transfer Division, (Publication) HTD, (1991) 15-23.
[31] L.M. Tam, A.J. Ghajar, Transitional heat transfer in plain horizontal tubes, Heat Transfer Engineering, 27(5) (2006) 23-38.
[32] A.J. Ghajar, L.M. Tam, Flow regime map for a horizontal pipe with uniform wall heat flux and three inlet configurations, Experimental Thermal and Fluid Science, 10(3) (1995) 287-297.
[33] A.J. Ghajar, L.M. Tam, S.C. Tam, Improved heat transfer correlation in the transition region for a circular tube with three inlet configurations using artificial neural networks, Heat Transfer Engineering, 25(2) (2004) 30-40.
[34] M. Everts, J.P. Meyer, Relationship between pressure drop and heat transfer of developing and fully developed flow in smooth horizontal circular tubes in the laminar, transitional, quasi-turbulent and turbulent flow regimes, International Journal of Heat and Mass Transfer, 117 (2018) 1231-1250.
[35] J.P. Meyer, S.M. Abolarin, Heat transfer and pressure drop in the transitional flow regime for a smooth circular tube with twisted tape inserts and a square-edged inlet, International Journal of Heat and Mass Transfer, 117 (2018) 11-29.

[36] J.P. Meyer, M. Everts, A.T.C. Hall, F.A. Mulock-Houwer, M. Joubert, L.M.J. Pallent, E.S. Vause, Inlet tube spacing and protrusion inlet effects on multiple circular tubes in the laminar, transitional and turbulent flow regimes, International Journal of Heat and Mass Transfer, 118 (2018) 257-274.
[37] J. Dirker, J.P. Meyer, D.V. Garach, Inlet flow effects in micro-channels in the laminar and transitional regimes on single-phase heat transfer coefficients and friction factors, International Journal of Heat and Mass Transfer, 77 (2014) 612-626.
[38] M. Everts, J.P. Meyer, Flow regime maps for smooth horizontal tubes at a constant heat flux, International Journal of Heat and Mass Transfer, 117 (2018) 1274-1290.
[39] A.I. Bashir, M. Everts, J.P. Meyer, Influence of inlet contraction ratios on the heat transfer and pressure drop characteristics of single-phase flow in smooth circular tubes in the transitional flow regime, Experimental Thermal and Fluids Science, Manuscript nr: ETFS_2019_412, Submitted on 22 March 2019 (2019).
[40] J.P. Meyer, T.J. McKrell, K. Grote, The influence of multi-walled carbon nanotubes on single-phase heat transfer and pressure drop characteristics in the transitional flow regime of smooth tubes, International Journal of Heat and Mass Transfer, 58(1-2) (2013) 597-609.
[41] J.P. Meyer, J.A. Olivier, Heat transfer and pressure drop characteristics of smooth horizontal tubes in the transitional flow regime, Heat Transfer Engineering, 35(14-15) (2014) 1246-1253.
[42] J.P. Meyer, J.A. Olivier, Heat transfer and pressure drop characteristics of circular smooth tubes in the transitional flow regime, in: 19th International Congress of Chemical and Process Engineering, CHISA 2010 and 7th European Congress of Chemical Engineering, ECCE-7, 2010.
[43] D.D. Ndenguma, J. Dirker, J.P. Meyer, Transitional flow regime heat transfer and pressure drop in an annulus with non-uniform wall temperatures, International Journal of Heat and Mass Transfer, 108 (2017) 2239-2252.
[44] J.A. Olivier, J.P. Meyer, Single-phase heat transfer and pressure drop of the cooling of water inside smooth tubes for transitional flow with different inlet geometries (RP-1280), HVAC&R Research, 16(4) (2010) 471-496.
[45] D.D. Ndenguma, J. Dirker, J.P. Meyer, Heat transfer and pressure drop in annuli with approximately uniform internal wall temperatures in the transitional flow regime, International Journal of Heat and Mass Transfer, 111 (2017) 429-441.
[46] J.P. Meyer, J.A. Olivier, Transitional flow inside enhanced tubes for fully developed and developing flow with different types of inlet disturbances: Part II – Heat transfer, International Journal of Heat and Mass Transfer, 54(7-8) (2011) 1598-1607.
[47] J.P. Meyer, J.A. Olivier, Transitional flow inside enhanced tubes for fully developed and developing flow with different types of inlet disturbances: Part I – Adiabatic pressure drops, International Journal of Heat and Mass Transfer, 54(7) (2011) 1587-1597.
[48] A. Bejan, S. Lorente, L. Martins, J.P. Meyer, The constructal size of a heat exchanger, Journal of Applied Physics Journal of Applied Physics, 122(6) (2017) 064902.
[49] S.M.A. Noori Rahim Abadi, J.P. Meyer, J. Dirker, Effect of inclination angle on the condensation of R134a inside an inclined smooth tube, Chemical Engineering Research and Design, 132 (2018) 346-357.
[50] M. Mahdavi, M. Sharifpur, J.P. Meyer, Exploration of nanofluid pool boiling and deposition on a horizontal cylinder in Eulerian and Lagrangian frames, International Journal of Heat and Mass Transfer, 125 (2018) 959-971.
[51] M. Everts, Heat transfer and pressure drop of developing flow in smooth tubes in the transitional flow regime, Masters dissertation, University of Pretoria, Pretoria, 2014.

[52] A. Bakker, R.D. LaRoche, E.M. Marshall, Laminar flow in static mixers with helical elements, in: The Online CFM Book (2000).
[53] M. Everts, Single-phase mixed convection of developing and fully developed flow in smooth horizontal circular tubes in the laminar, transitional, quasi-turbulent and turbulent flow regimes, PhD thesis, University of Pretoria, Pretoria, 2018.
[54] K.H. Tam, L.M. Tam, A.J. Ghajar, Effect of inlet geometries and heating on the entrance and fully-developed friction factors in the laminar and transition regions of a horizontal tube, Experimental Thermal and Fluid Science, 44 (2013) 680-696.
[55] R.E. Rayle, Influence of orifice geometry on static pressure measurements, ASME paper No 59-A-234, (1959).
[56] H.A. Mohammed, Laminar mixed convection heat transfer in a vertical circular tube under buoyancy-assisted and opposed flows, Energy Conversion and Management, 49 (2008) 2006-2015.
[57] D.D. Joye, Comparison of correlations and experiment in opposing flow , mixed convection heat transfer in a vertical tube with Grashof number variation, International Journal of Heat and Mass Transfer, 39(5) (1996) 1033-1038.
[58] P.E. Saylor, D.D. Joye, Hydrostatic correction and pressure drop measurement in mixed convection heat transfer in a vertical tube, Industrial & Engineering Chemistry Research, 30(4) (1991) 784-788.
[59] C.O. Popiel, J. Wojtkowiak, Simple formulas for thermophysical properties of liquid water for heat transfer calculations (from 0°C to 150°C), Heat Transfer Engineering, 19(3) (1998) 87-101.
[60] C. Wang, P. Gao, S. Tan, Z. Wang, C. Xu, Experimental study of friction and heat transfer characteristics in narrow rectangular channel, Nuclear Engineering and Design, 250(0) (2012) 646-655.
[61] C. Wang, P. Gao, S. Tan, Z. Wang, Forced convection heat transfer and flow characteristics in laminar to turbulent transition region in rectangular channel, Experimental Thermal and Fluid Science, 44 (2013) 490-497.
[62] J. Ma, L. Li, Y. Huang, X. Liu, Experimental studies on single-phase flow and heat transfer in a narrow rectangular channel, Nuclear Engineering and Design, 241(8) (2011) 2865-2873.
[63] T.S. Zhao, Q.C. Bi, Pressure drop characteristics of gas–liquid two-phase flow in vertical miniature triangular channels, International Journal of Heat and Mass Transfer, 44(13) (2001) 2523-2534.
[64] F. Madrid, N. Caney, P. Marty, Study of a vertical boiling flow in rectangular mini-channels, Heat Transfer Engineering, 28(8-9) (2007) 753-760.
[65] M.V. Sardeshpande, P. Shastri, V.V. Ranade, Two-phase flow boiling pressure drop in small channels, International Journal of Heat and Fluid Flow, 61 (2016) 636-649.
[66] P.F. Dunn, Measurement and Data Analysis for Engineering and Science, 2nd ed., CRC press, United States of America, 2010.
[67] J.L. Poiseuille, Recherches expérimentales sur le mouvement des liquides dans les tubes de très- petits diamètres, Imprimerie Royale, (1844).
[68] H. Blasius, Das ähnlichkeitsgesetz bei reibungsvorgangen in flüssigkeiten, Forschg. Arb. Ing.-Wes, (1913) 131-137.
[69] S.M. Morcos, A.E. Bergles, Experimental investigation of combined forced and free laminar convection in horizontal tubes, Journal of Heat Transfer, 97(2) (1975) 212-219.

[70] V. Gnielinski, New equations for heat and mass-transfer in turbulent pipe and channel flow, International Chemical Engineering, 16(2) (1976) 359-368.
[71] J.P. Meyer, M. Everts, N. Coetzee, K. Grote, M. Steyn, Heat transfer coefficients of laminar, transitional, quasi-turbulent and turbulent flow in circular tubes, International Communications in Heat and Mass Transfer, 105 (2019) 84-106.
[72] A.I. Bashir, M. Everts, J.P. Meyer, R. Bennacer, Single-phase forced convection heat transfer and pressure drop in circular tubes in the laminar and transitional flow regimes, Experimental Thermal and Fluids Science, Manuscript nr: ETFS_2019_411, Submitted on 22 March 2019 (2019).
[73] S.V. Patankar, Numerical Heat Transfer and Fluid Flow, Hemisphere Publ. Corp., Washington, DC, 1985.
[74] K.C. Rolle, Heat and Mass Transfer, Cengage Learning, Boston, 2016.